remote sensing

MDPI

Article

Impacts of Land-Use Change on the Spatio-Temporal Patterns of Terrestrial Ecosystem Carbon Storage in the Gansu Province, Northwest China

Lingge Wang [1], Rui Zhu [1], Zhenliang Yin [2,*], Zexia Chen [1], Chunshuang Fang [1], Rui Lu [1], Jiqiang Zhou [3,4] and Yonglin Feng [3,4]

[1] Faculty of Geomatics, National-Local Joint Engineering Research Center of Technologies and Applications for National Geographic State Monitoring, Gansu Provincial Engineering Laboratory for National Geographic State Monitoring, Lanzhou Jiaotong University, Lanzhou 730000, China; 11200865@stu.lzjtu.edu.cn (L.W.); zhur@mail.lzjtu.cn (R.Z.); 12201841@stu.lzjtu.edu.cn (Z.C.); 12211915@stu.lzjtu.edu.cn (C.F.); 12211933@stu.lzjtu.edu.cn (R.L.)
[2] Key Laboratory of Ecohydrology of Inland River Basin, Northwest Institute of Eco-Environment and Resources, Chinese Academy of Sciences, Lanzhou 730000, China
[3] Technology Innovation Center for Mine Geological Environment Rehabilitation Engineering in Alpine and Arid Regions, Ministry of Natural Resources, Lanzhou 730000, China; xbyl0000@163.com (J.Z.); fylcxzx@163.com (Y.F.)
[4] Gansu Nonferrous Engineering Survey, Design and Research Institute, Lanzhou 730000, China
* Correspondence: yinzhenliang@lzb.ac.cn

Abstract: Land-use change is supposed to exert significant effects on the spatio-temporal patterns of ecosystem carbon storage in arid regions, while the relative size of land-use change effect under future environmental change conditions is still less quantified. In this study, we combined a land-use change dataset with a satellite-based high-resolution biomass and soil organic carbon dataset to determine the role of land-use change in affecting ecosystem carbon storage from 1980 to 2050 in the Gansu province of China, using the MCE-CA-Markov and InVEST models. In addition, to quantify the relative size of the land-use change effect in comparison with other environmental drivers, we also considered the effects of climate change, CO_2 enrichment, and cropland and forest managements in the models. The results show that the ecosystem carbon storage in the Gansu province increased by 208.9 ± 99.85 Tg C from 1980 to 2020, 12.87% of which was caused by land-use change, and the rest was caused by climate change, CO_2 enrichment, and ecosystem managements. The land-use change-induced carbon sequestration was mainly associated with the land-use category conversion from farmland to grassland as well as from saline land and desert to farmland, driven by the grain-for-green projects in the Loess Plateau and oasis cultivation in the Hexi Corridor. Furthermore, it was projected that ecosystem carbon storage in the Gansu province from 2020 to 2050 will change from −14.69 ± 12.28 Tg C to 57.83 ± 53.42 Tg C (from 105.62 ± 51.83 Tg C to 177.03 ± 94.1 Tg C) for the natural development (ecological protection) scenario. By contrast, the land-use change was supposed to individually increase the carbon storage by 56.46 ± 9.82 (165.84 ± 40.06 Tg C) under the natural development (ecological protection) scenario, respectively. Our results highlight the importance of ecological protection and restoration in enhancing ecosystem carbon storage for arid regions, especially under future climate change conditions.

Keywords: land-use change; carbon density dynamics; satellite-based carbon datasets; MCE-CA-Markov; InVEST; arid regions

Citation: Wang, L.; Zhu, R.; Yin, Z.; Chen, Z.; Fang, C.; Lu, R.; Zhou, J.; Feng, Y. Impacts of Land-Use Change on the Spatio-Temporal Patterns of Terrestrial Ecosystem Carbon Storage in the Gansu Province, Northwest China. *Remote Sens.* **2022**, *14*, 3164. https://doi.org/10.3390/rs14133164

Academic Editor: Damiano Gianelle

Received: 6 May 2022
Accepted: 27 June 2022
Published: 1 July 2022

1. Introduction

With the increasing emissions of carbon dioxide since the onset of industrialization, greenhouse gas (GHG) concentration in the atmosphere has soared, resulting in global climate change and a series of environmental issues, threatening ecosystems' health and

social and economic development [1–3]. In 2016, the Paris Agreement reached a political consensus that global warming should not exceed 2 °C or 1.5 °C [4–6]. The Intergovernmental Panel on Climate Change (IPCC) Special Report on Global Warming of 1.5 °C, which was released in 2018, once again highlighted that the limiting of global warming to 1.5 °C rather than 2 °C could avoid a series of climate change impacts (such as the 10 cm reduction in sea level rising and higher survival rates of coral reefs) [7,8]. Moreover, this special report also placed a demand on the rapid and far-reaching transition across industries in countries around the world [9]. Notably, as the world's largest developing country and carbon dioxide (CO_2) emitter [10], China's rapid economic development also resulted in massive energy consumption. Accordingly, the Chinese government proposed the goals of "2030 carbon peak" and "2060 carbon neutrality" [11,12], which called for lower carbon emissions and stronger carbon storage (CS) capacity. Enhancing the carbon storage of ecosystems is considered as one of the most economically viable and environmentally friendly ways to mitigate the greenhouse effect and climate change [10,13,14]. As an ecological province in the arid region of northwest China, the Gansu province is characterized by complex landscapes, diverse ecosystem types, and large potential carbon sequestration capacity, acting as an important region to achieve China's goals of "carbon peak" and "carbon neutrality".

The terrestrial ecosystem CS are mainly divided into four major carbon pools (aboveground biomass carbon pool, below-ground biomass carbon pool, soil organic carbon pool, and dead organic matter carbon pool) [2,15,16]. The land use/cover change (LUCC) is an essential feature reflecting environmental changes [17] and a prime influencing factor of terrestrial ecosystem carbon storage [18,19]. Therefore, it is of great significance to quantify the effects of land-use change on ecosystem CS under climate change over the past and in the future [20]. Leh et al. [21] used the InVEST (Integrated Valuation of Ecosystem Services and Trade-offs) model to quantify the land-use change effects on CS in west Africa. Dargains and Cabral [22] evaluated the CS on a cattle ranch from 2007 to 2017 and then created four alternative land-use scenarios with the InVEST Scenario Generator for 2027 to simulate LUCC and forecast future CS dynamics. Wang et al. [10] constructed an urban-level framework of future LUCC and CS simulation under the context of CMIP6 climate change scenarios, integrating system dynamics (SD) model, patch-generating land use simulation (PLUS) model, and the InVEST model. It can be found that more and more studies have been focusing on future carbon storage dynamics, especially the impact of future land-use type conversion (LUTC) on carbon storage. Previous studies generally assumed that the biomass and soil organic carbon density were constant during the quantification of ecosystem carbon storage dynamics over time by the InVEST model. However, under the background of global climate change, the changes in climatic factors, atmospheric CO_2 concentrations, and managements practices can also exert large effects on vegetation growth and soil respiration, and further alter the vegetation biomass and soil organic carbon density, even the land-use category keeps constant. Thus, to quantify the relative size of the land-use change effect in comparison with other environmental drivers, the effects of climate change, CO_2 enrichment, and cropland and forest managements on biomass and soil organic carbon density should also be considered in the InVEST model.

There are many types of models used to simulate and predict the evolution of future land-use patterns, among which the CA-Markov [23,24], FLUS [25–27], PLUS [28,29], CLUMondo [30], and CLUE-S [31,32] are widely employed. Taking the Shiyang River Basin in the arid region of northwest China as an example, Wang et al. [19] concluded that the LR-CA-Markov and FLUS models performed better in the arid region than other land-use simulation models. The CA-Markov model has been widely used in many fields, such as land use, urban growth, and diffusion in arid regions [33,34]. The model integrates the ability of the Cellular Automata (CA) model in simulating the spatial changes of complex systems and the advantages of the Markov model in long-term prediction. It can effectively simulate the spatial change in land-use pattern and improve the accuracy of land-use type conversion prediction, with good scientificity and practicality [35,36]. Based on the

LUCC patterns of east Nepal during 1989–2016, Rimal et al. [37] used the CA-Markov to predict the urban expansion from 2026 to 2036 and found that the area of dry farmland was supposed to continuously shrink in future, implying that food security crisis and environmental degradation may occur in this region. Mokarram et al. [34] employed the CA-Markov combined with 12 parameters to predict the drought map of Fars in Iran for 2030 and 2040, which demonstrated that the drought index would continue to increase and the way of local farming should change over time to cope with the increasingly dry climate. Along with the speeding up of ecological construction, China has implemented a series of ecological protection projects, such as the grain for green, degraded grasslands restoration, desertification controls, and soil erosion prevention. Therefore, the simulation of future land use needs to consider the ecological protection scenario (EPS) and compare it with the spatial pattern of land use under the natural development scenario (NDS) to explore the characteristics of the spatial and temporal dynamics of carbon storage under the two scenarios, so as to provide a reference for policy makers.

The carbon storage estimations at a regional scale mostly rely on the carbon density data of different land-use types derived from site-level measurements or the published literature. However, due to the large spatial heterogeneity of biomass and soil organic carbon density, limited site-level measurements may not fully capture the high variability of carbon even within the same land-use type over space, leading to uncertainties in the carbon storage change estimations [38,39]. Hence, it is needed to obtained biomass and soil carbon datasets with high-spatial resolution and quality for the evaluation of ecosystem carbon dynamics [40]. Over the past decade, with the rapid development of remote sensing and machine learning techniques, increasing aboveground and belowground biomass as well as soil organic carbon density maps were created based on a large amount of field measurements and satellite-derived covariates. The commonly used soil organic carbon dataset included the SoilGrids 250 m product, which was seemed to be quite coarse in resolution and quality for regional studies. Recently, Liu et al. [41] developed soil organic carbon gridded datasets at a resolution of 90 m in China based on the digital soil mapping framework, which used remote-sensing-derived spectral indexes and other climatic, topographic, and pedologic covariates to predict the spatial distribution of soil organic carbon at a national scale. However, the efficiency of this satellite-based carbon products in quantifying the spatio-temporal dynamics of ecosystem carbon storage as affected by land-use change is still less evaluated, especially in regions such as the Gansu province being characterized by complex landscapes. In addition, most of the previous studies concerning the land-use change effects on ecosystem carbon storage dynamics only considered the historical changes, while the impact of future evolution of LUCC on carbon storage should be considered in terms of ecosystem carbon management under future climate change conditions.

Therefore, based on the sub-categories of LUCC from 1980 to 2020 and the high-precision carbon density dynamic data of the Gansu province, this study firstly analyzed the changing characteristics of land use in the historical period (Section 3.1) and discussed the terrestrial ecosystem carbon storage changes as affected by land-use change and other environmental drivers (Section 3.2). Secondly, the MCE-CA-Markov model was used to predict the spatial distribution of land use in 2030 and 2050 under NDS and EPS scenarios, and the spatial patterns of terrestrial ecosystem carbon storage by 2030 and 2050 under land-use change scenarios (NDS and EPS) and future climate change scenarios were analyzed (Section 3.3). Finally, the relationship between land-use changes and terrestrial ecosystem carbon storage changes was discussed (Section 4) to provide suggestions for future land use and carbon management in arid regions, and for effectively managing ecosystem carbon pools under future climate change.

2. Materials and Methods

2.1. Study Area

The Gansu province is located in the inland hinterland of Northwest China, ranging from 32°11′ to 42°57′N in latitude and 92°13′ to 108°46′E in longitude, with a total area of 45.59 × 10^4 km^2 (Figure 1). The geographical shape of Gansu is narrowly distributed in the northwest to southeast direction, with a length of 1659 km from east to west and a width of 530 km from north to south. Moreover, the Gansu province is located at the intersection of three main plateaus of China (i.e., the Loess Plateau, Qinghai-Tibet Plateau, and Inner Mongolia Plateau) [42], with a wide range of elevations ranging from 1000 to 3000 m. In addition, the spatial distribution of precipitation in the Gansu province is uneven, which decreases from southeast to northwest with annual means ranging from 40 to 800 mm [43], creating very fragmented landscapes and diverse types of ecosystems, leading to different land-use types from east to west of the Gansu province. The western part is the Hexi Corridor being characterized by a desert-oasis landscape due to dry climate, scarce precipitation, and strong evapotranspiration [44]. The eastern part includes the Gannan Plateau and part of the Loess Plateau, with complex landform types (dominates by mountains and hills) and rich forest and grass resources.

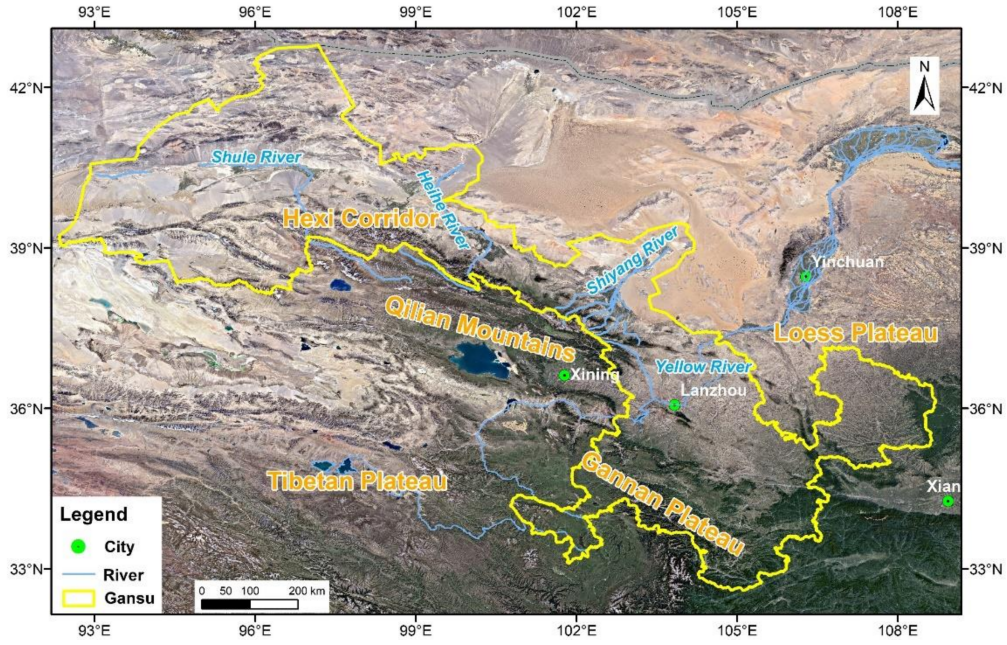

Figure 1. Geographical location of the Gansu province.

2.2. Data Sources

2.2.1. Land-Use Data

The land-use data of Gansu province used in this study were obtained from the National Land-Use/Cover Database of China (NLUD-C) on the Resource and Environment Science Data Center of the Chinese Academy of Sciences (RESDC) (https://www.resdc.cn, accessed on 6 October 2021), which were interpreted based on Landsat-MSS, Landsat-TM, and Landsat 8 images with the human–machine interaction method. Through random verification at the field surveys, the accuracy of LUCC interpretation was more than 90% [40,45], which meet the experimental requirements. After that, the land-use types in the Gansu province were classified with reference to the National Ecological Remote Sensing Monitoring Land Use/Land Cover Classification System. As the area of paddy fields in the Gansu province only accounts for 0.05% of the total area, it was combined with drylands as dry farmland. In addition, related research results have shown that the carbon density of water is close to 0 [30,46,47]. Therefore, the land-use types of water, such as lakes

and permanent glacials, were classified and combined into river and glacier in this study. Finally, the land types of the Gansu province were divided into 19 land-use types.

2.2.2. Satellite-Derived Carbon Maps

In this study, the datasets being employed to estimate carbon storage primarily included vegetation carbon density (above- and below-ground biomass), soil carbon density, and dead organic matter carbon density (Figures 2 and S1). The carbon density data of above- and below-ground biomass were provided by Spawn and Gibbs [48], who published the earth datasets in the National Aeronautics and Space Administration (NASA) Oak Ridge National Laboratory Distributed Active Archive Center (ORNL DAAC) with 300 m resolution in 2020. Maps reporting the accumulated uncertainty of pixel-level biomass carbon density estimates were also provided. The uncertainty here represents the cumulative standard error, which was propagated through the harmonization process using summation in quadrature [48]. The soil carbon density was extracted from the Chinese High-Resolution National Soil Information Grid Basic Dataset, which was published by Liu et al. [41] on the National Earth System Science Data Center (http://soil.geodata.cn/data/datadetails.html?dataguid=36810085119113, accessed on 18 October 2021). This soil dataset with a 90 m resolution of multi-properties was generated by integrating efficient machine learning techniques with predictive soil mapping paradigms in a high-performance computing environment, with soil environmental characterization information obtained from remote sensing data processing. These datasets also provided uncertainty maps of SOC content and bulk density, which could be further used to quantify the uncertainties of SOC storage in this study under different climate and land-use change scenarios. The uncertainty of initial soil predictions, being expressed as upper and lower limits of 90% prediction interval, was simultaneously estimated at every pixel and depth based on bootstrap method. The limits were identified using the 0.05 and 0.95 quantiles of empirical distribution. To facilitate comparison with the uncertainty of vegetation biomass carbon density, we further converted the initial quantile interval of soil predictions to standard error based on their statistical relationships and used the standard error as the uncertainty of SOC in this study (Figure S1).

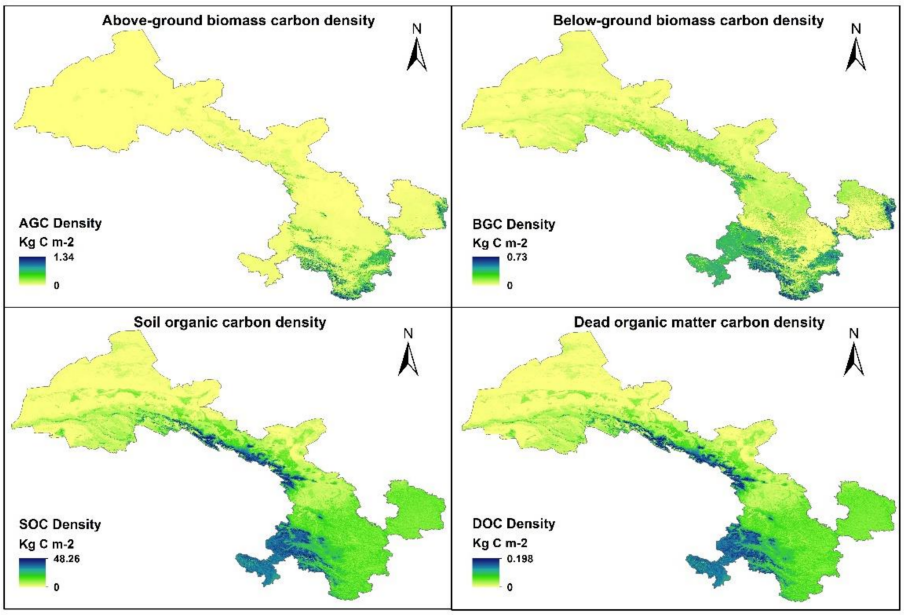

Figure 2. Spatial distribution of terrestrial ecosystem carbon density of the Gansu province.

The soil carbon density data used in this study were soil organic carbon density at 0–100 cm (Figures 2 and S1), which were obtained by multiplying the SOC content at 0–5,

5–15, 15–30, 30–60, and 60–100 cm with the corresponding bulk density at each layer from the dataset according to the following equations:

$$SOCD = \sum_{i}^{n} SOCC_i \times BD_i \times D_i \quad (1)$$

where SOCD is the density of soil origin carbon (kg C m^{-2}), n is the count of layers, $SOCC_i$ is the concentration of soil organic carbon (g C kg^{-1}), and BD_i and D_i denote the bulk density (g cm^{-3}) and the depth (m), respectively. The dead organic carbon density (DOC) for the Gansu province was obtained by an empirical equation (Figure 2). We first regressed the linear relationships between SOC and DOC in the Gansu province ($y = 0.0041x + 5.1899$, $R^2 = 0.6897$) based on the 50 km resolution dataset of "A dataset of organic carbon storage and carbon dynamic in arid and semiarid China from 1980 to 2014", which was provided by Fang et al. [49] (https://www.scidb.cn/en/detail?dataSetId=633694461100032002, accessed on 3 January 2022). Then, we obtained the DOC maps of the Gansu province by applying the equation to the SOC maps.

2.2.3. Environmental Variables

In the simulation of future land-use scenarios, the relationships between environmental variables and land types need to be separately explored according to regional characteristics. In this study, the types of spatial datasets can be divided into topography, climate, and human activity. The driving factors may not be enumerated utterly, but the aggregation of the land-use simulations can be improved from multiple perspectives. The list of data is as follows (Table 1).

Table 1. Datasets used in this study.

Type	Variables	Original Resolution	Source
LUCC	Land-use map in 1980, 2000 and 2020	1:100,000	https://www.resdc.cn, accessed on 6 October 2021
Carbon	Above-ground biomass carbon	300 m	Spawn et al. [50]
	Below-ground biomass carbon	300 m	https://daac.ornl.gov/cgi-bin/dsviewer.pl?ds_id=1763, accessed on 18 October 2021
	SOC content at 0–5, 5–15, 15–30, 30–60, and 60–100 cm	90 m	Liu et al. [41] http://soil.geodata.cn/data/datadetails.html?dataguid=36810085119113, accessed on 18 October 2021
	Bulk density at 0–5, 5–15, 15–30, 30–60, and 60–100 cm	90 m	
	Carbon dynamics in arid and semiarid China from 1980 to 2014	50 km	https://www.scidb.cn/en/detail?dataSetId=633694461100032002, accessed on 3 January 2022
Topography	Elevation	30 m	ASTER GDEM (https://earthdata.nasa.gov/, accessed on 3 January 2022)
	Aspect	30 m	Calculated by SAGA GIS
	Slope	30 m	Calculated by SAGA GIS
	Topographic wetness	30 m	Calculated by SAGA GIS
	Multi-scale topographic position	30 m	Calculated by SAGA GIS
Climate	Historical and future temperature	1000 m	Peng et al. [51–58] https://data.tpdc.ac.cn/zh-hans/data/71ab4677-b66c-4fd1-a004-b2a541c4d5bf/, accessed on 3 January 2022 https://data.tpdc.ac.cn/zh-hans/data/7f0fce77-2cba-4bdc-ab02-b2d7c69e8e4b/, accessed on 3 January 2022
	Historical and future precipitation	1000 m	Peng et al. [51–58] https://data.tpdc.ac.cn/zh-hans/data/faae7605-a0f2-4d18-b28f-5cee413766a2/, accessed on 3 January 2022 https://data.tpdc.ac.cn/zh-hans/data/a9cd4a09-51a9-433b-9540-0376c6134cf6/, accessed on 3 January 2022
CO_2 concentrations	Historical and future concentrations of CO_2	0.5°	https://greenhousegases.science.unimelb.edu.au/#!/ghg?mode=downloads, accessed on 7 February 2022
Human activity	River network density	1:1 million	National Basic Geographic Database (2015) (https://mulu.tianditu.gov.cn/, accessed on 1 October 2021)
	Road density	1:1 million	
	Population	1000 m	Chinese Academy of Sciences (2015) (http://www.resdc.cn/, accessed on 1 October 2021)
	Gross domestic product	1000 m	

2.3. LUCC Modelling

The MCE-CA-Markov model consists of a CA filter, Markov chain, and MCE module [59]. The MCE module uses limiting and driving factors as independent variables to

establish an atlas of land-use change suitability rules for each category, providing a decision aid for the change in future land use. CA-Markov based on the MCE module can not only improve the simulation accuracy, but also be more reliable for LUCC simulation results in future projections [60]. CA filter is a discrete model in time and space, and each cell of the CA filter is affected both by neighboring cells and its own changes in cell characteristics. Because of the presumed ability of the CA filter in simulating the spatio-temporal evolution of complex spatial patterns, it is widely used in the study of land-use simulation, population migration, and urbanization. The CA model can be expressed by the following equation:

$$S_{t1} = f(S_t, N) \quad (2)$$

where S is the set of cellular states, t and t1 are the moments before and after the cellular is located (respectively), f is the transition rule, and N is the cellular neighborhood.

The Markov chain is a method to predict the probability of event occurrence based on the transfer probability matrix. The transfer probability matrix is only related to the states of periods t_0 and t_1. The expressions are as follows.

$$S_{t1} = P_{ij} \cdot S_t \quad (3)$$

$$P_{ij} = \begin{bmatrix} P_{11} & P_{12} & \cdots & P_{1n} \\ P_{21} & P_{22} & \cdots & P_{2n} \\ \vdots & \vdots & \vdots & \vdots \\ P_{n1} & P_{n2} & \cdots & P_{nn} \end{bmatrix} \quad (4)$$

where S_t and S_{t1} are the land use of periods t and t1, P_{ij} is the transfer probability matrix, n is the land-use type, and i, j = 1, 2, . . . , n represents the land-use types before and after the transfer, respectively.

In this study, based on the MCE-CA-Markov model of the IDRISI Selva 17.0 platform, the simulated land-use data of the Gansu province in 2020 were predicted with a period of 10 and 20 years to compare with the actual data of 2020 to verify the simulation reliability of MCE-CA-Markov. After that, the land-use data in 2030 was predicted with 2020 as the base period, and then the spatial distribution data of land use in 2050 was predicted with 2030 as the start year. The main steps were as follows: (1) Production of suitability atlas. According to the requirements of unique geographical conditions and the land resource conservation of the Gansu province, the MCE module was used to set restrictive factors (including dry farmland, woodland, grassland, water, and unused land) and impact factors (including 11 driving factors of topography, climate, human activity, and default suitability atlas) for each land types. (2) Land-use prediction of future. The number of CA filter cycles was set to 10 for predicting the 2030 land-use distribution based on the 2020 land-use data. Similarly, the number of cycles was set to 20 for predicting the 2050 land-use distribution based on the land use of 2030.

To determine the effects of the ecological conservation policies implementation on LUCC and CS, this study set two possible land-use change scenarios and the corresponding constraints. Scenario 1: Natural development scenario (NDS), which assumed that the trend of LUTC from 2020 to 2030 was consistent with the change from 2010 to 2020, the actual 2020 was used as the base year to simulate 2030. It was also assumed that the change from 2030 to 2050 was consistent with the change from 2010 to 2030, so that 2030 was used as the starting year to simulate 2050. Scenario 2: Ecological protection scenario (EPS), which referred to the policy of grain for green, the Ecological Protection and Construction Plan of Gansu province (2014–2020), the 14th Five-Year Plan for National Economic and Social Development of Gansu province, the Outline of Long-Term Goals in 2035, and other ecological protection documents. For the EPS, strict controls were implemented on the transfer out of each land use type, and a new suitability image for each land use was generated together with the 11 impact factors and the suitability image generated by

default as impact factors. Then, the transformation probability matrix was modified in a certain proportion to better meet the policy requirements.

The accurate 2020 land-use map of the Gansu province was used as the baseline to verify the simulation accuracy in 2020 under NDS and EPS with the period of 10- and 20-year cycle, respectively. The simulated kappa coefficients for 2020 are all greater than 0.9, FoM (Figure of Merit) coefficient is larger than 0.25, indicating that the MCE-CA-Markov model can be used to predict the future land-use patterns of the Gansu province.

2.4. InVEST Model

The Carbon module of the InVEST model divides the carbon storage of ecosystems into four basic carbon pools [35,61]: above-ground biomass carbon (AGC: carbon in all surviving plants above the soil), below-ground biomass carbon (BGC: carbon present in living root system of plants), soil organic carbon (SOC: organic carbon distributed in organic and mineral soils), and dead organic matter carbon (DOC: carbon in dead plants and fallen matter) [62]. The carbon storage of the cell (i, j) can be calculated by its corresponding land-use carbon density [22].

$$CS_{m,i,j} = A \times \left(Ca_{m,i,j} + Cb_{m,i,j} + Cs_{m,i,j} + Cd_{m,i,j}\right) \quad (5)$$

where $CS_{m,i,j}$ is the carbon storage (t) of a given cell (i, j), and A is the actual area of a single cell. $Ca_{m,i,j}$, $Cb_{m,i,j}$, $Cs_{m,i,j}$, and $Cd_{m,i,j}$ are AGC, BGC, SOC, and DOC carbon density (t ha^{-1}) of land-use type m, respectively. The InVEST model assumes that the carbon density of each land-type is constant over time, and this assumption may bring uncertainties to the estimation of ecosystem carbon storage at a decadal scale. To consider the effects of climate change and vegetation growth on carbon sequestration capacity, we deduced past and future AGC, BGC, SOC, and DOC dynamics based on empirical equations (Tables S1 and S2). The detailed procedure and results of carbon density estimation at different periods can be found in Supplementary Materials (Tables S3–S6). The mean values of terrestrial ecosystem carbon density (sum of above- and below-ground biomass, soil carbon and dead organic carbon density) corresponding to land-use types in different periods are shown in Table 2. The carbon storage and its uncertainty for each period and scenario were also estimated in the InVEST model by integrating both the mean and uncertainty of carbon density to the land-use dataset.

Table 2. The mean carbon densities of terrestrial ecosystem across the Gansu province of historical periods (1980, 2000, and 2020) and future periods (2030 and 2050) under SSP126, SSP245, and SSP585 scenarios. Note: SSP represents the shared socio-economic pathways in CMIP6 models.

Top-Level Categories	Sub-Categories	Mean Carbon Densities of Terrestrial Ecosystem (kg C m^{-2})								
		1980	2000	2020	SSP126		SSP245		SSP585	
					2030	2050	2030	2050	2030	2050
Farmland	Dry farmland	9.72	9.36	9.51	9.48	9.52	9.51	9.45	9.47	9.36
Forest	Wood land	20.76	21.26	23.41	23.44	24.00	23.50	24.07	23.47	24.10
	Shrubbery land	19.42	19.76	21.36	21.28	21.57	21.35	21.65	21.32	21.69
	Sparsely forested woodland	13.47	13.97	16.32	16.40	17.09	16.46	17.04	16.42	17.06
	Other forest land	15.22	14.17	14.71	13.95	13.19	13.99	12.91	13.92	12.71
Grassland	High coverage grassland	20.66	19.39	20.20	19.57	18.76	19.61	18.72	19.60	18.84
	Middle coverage grassland	12.36	11.34	12.44	12.11	11.75	12.12	11.62	12.12	11.77
	Low coverage grassland	6.25	6.04	6.64	6.60	6.53	6.63	6.63	6.64	6.84
Water	River and glacier	0.00	0.00	0.00	0.00	0.00	0.00	0.00	0.00	0.00
Built-up land	Cities and towns	6.46	6.23	6.38	6.21	5.96	6.23	6.01	6.23	6.07
	Rural settlements	9.96	9.46	9.37	8.94	8.38	8.97	8.34	8.94	8.27
	Industry and traffic land	5.89	5.50	5.84	5.56	5.19	5.58	5.17	5.56	5.21
Unused land	Sandy land	1.76	1.89	2.31	2.35	2.35	2.38	2.53	2.40	2.69
	Gobi	1.81	1.82	2.09	2.07	2.00	2.10	2.14	2.11	2.25
	Saline-alkali land	3.47	3.33	3.24	3.06	2.75	3.10	2.91	3.10	2.99
	Swampland	16.80	16.13	16.76	16.56	16.18	16.65	16.62	16.71	17.10
	Bare land	3.31	3.23	3.54	3.46	3.33	3.49	3.43	3.49	3.54
	Rock and gravel	2.55	2.64	3.15	3.22	3.22	3.26	3.48	3.28	3.71
	Alpine desert	0.54	1.26	3.20	4.23	5.42	4.24	5.95	4.36	6.71

3. Results

3.1. LUCC during 1980–2020

The land-use type in the Gansu province was characterized by Gobi, dry farmland, middle coverage grassland, low coverage grassland, and rock and gravel (Table 3), accounting for 16.99%, 15.21%, 14.17%, 13.35%, and 10.78% of the total area, respectively. The large areas of Gobi, rock and gravel, and low coverage grassland reflected the fragile ecological environment of the Gansu province with arid climate and scarce water resources. In 1980–2020, the areas of grasslands grew significantly, with an increase of 1517.58 km^2 in high and mid-coverage grasslands and a decrease of 1139.49 km^2 in low coverage grassland. The water area increased from 3470.22 km^2 to 3845.25 km^2 over the past four decades. The built-up land of the Gansu province also expanded considerably, with the total area increasing from 592.83 km^2 in 1980 to 2146.05 km^2 in 2020. Meanwhile, the dry farmland shrunk considerably, with a total shrinkage of 730.17 km^2 in 1980–2020. In addition, the unused land shrank from 172,845 km^2 in 1980 to 169,988.63 km^2 in 2020, with a decrease of 2856.73 km^2. Except for rock and gravel, which increased by 2612.88 km^2, the rest of the unused land types showed a decreasing trend.

Table 3. Land-use changes in the Gansu province from 1980 to 2020.

Top-Level Categories	Sub-Categories	Area (km^2)			
		1980	2000	2020	Change (1980–2020)
Farmland	Dry farmland	64,658.52	65,602.26	63,928.35	−730.17
Forest	Wood land	14,033.79	14,012.55	14,167.35	133.56
	Shrubbery land	16,022.97	15,820.65	16,255.62	232.65
	Sparsely forested woodland	7340.76	7237.08	7206.84	−133.92
	Other forest land	538.02	554.58	874.35	336.33
Grassland	High coverage grassland	25,864.74	25,809.66	26,488.44	623.7
	Middle coverage grassland	60,089.22	59,758.92	60,983.1	893.88
	Low coverage grassland	57,255.21	57,029.22	56,115.72	−1139.49
Water	River and glacier	3470.22	3297.96	3845.25	375.03
Built-up land	Cities and towns	370.62	407.07	904.77	534.15
	Rural settlements	2732.04	2945.43	3443.4	711.36
	Industry and traffic land	222.21	228.78	1241.28	1019.07
Unused land	Sandy land	28,889.91	28,842.21	28,120.41	−769.5
	Gobi	72,811.08	72,579.6	71,410.05	−1401.03
	Saline-alkali land	8339.13	8357.94	7575.75	−763.38
	Swampland	2612.16	2606.49	2519.6	−92.56
	Bare land	3945.69	3721.59	38,92.14	−53.55
	Rock and gravel	44,878.32	45,266.76	47,491.2	2612.88
	Alpine desert	11,369.07	11,364.75	8979.48	−2389.59

The Gansu province has a long and narrow geographical region with large differences in spatial distribution of LUCC (Figure 3a–c). The vegetation in the southeast was lush, dominated by forest, high coverage grassland and middle coverage grassland, while in the northwest, it was dominated by the Gobi and desert, with less precipitation. The dry farmland was mainly distributed in the oasis area of the Hexi Corridor and the southeast of Gansu province. Analyzed from the perspective of the spatial distribution of major LUTC (Figure 3d), in the southeast, the converted regions were mainly concentrated in middle coverage grassland, low coverage grassland, and dry farmland, while in the northwest, the conversion among rock and gravel, Gobi, and low coverage grassland was dominant.

From 1980 to 2000, there was less LUTC in the Gansu province, with 188 conversion types and 4446.09 km^2 shifted-outward area, only accounting for 1.05% of the total area of the province. Dry farmland, middle coverage grassland, low coverage grassland, and Gobi were the main land-use types of conversion (Figure 4), shifting outward 513.63 km^2 (11.55%), 717.21 km^2 (16.13%), 823.32 km^2 (18.52%), and 568.44 km^2 (12.79%), respectively. Among them, the dry farmland mainly converted into rural settlements with the transferred area of 204.48 km^2, while the high coverage grassland, middle coverage grassland, and low coverage grassland mostly converted into dry farmland, and Gobi mostly converted into rock and gravel. Other land types were relative stable, with fewer types and areas

of conversion. Between 2000 and 2020, the land-use types of the Gansu province shifted more frequently, with 322 conversion types and the area of 36898.4 km^2 (8.67% of the total area) transferred outward. The conversion areas of dry farmland, middle coverage grassland, and low coverage grassland were larger (Figure 4), of which dry farmland shifted outward by 8939.52 km^2, accounting for 24.23% of the shifted area. Additionally, most of the rural settlements were converted from dry farmland, with the converted area reaching 440.82 km^2.

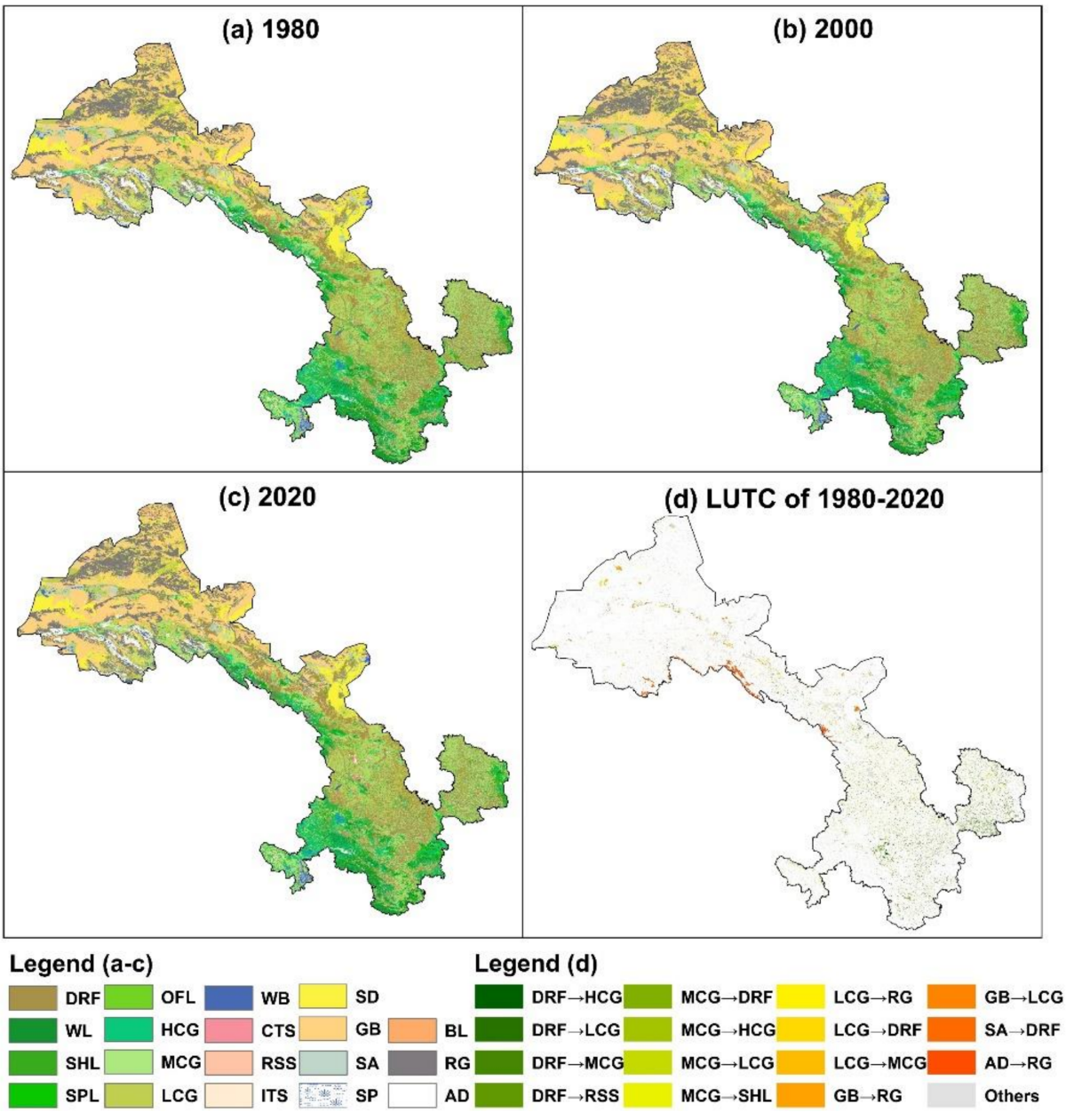

Figure 3. The spatial-distribution of LUCC (**a**–**c**) and LUTC (**d**) in Gansu from 1980 to 2020. DRF: dry farmland; WL: wood land; SHL: shrubbery land; SPL: sparsely forested woodland; OFL: other forest land; HCG: high coverage grassland; MCG: mid-coverage grassland; LCG: low coverage woodland; WB: river and glacier; CTS: cities and towns; RSS: rural settlements; ITS: industry and traffic land; SD: sandy land; GB: Gobi; SA: saline-alkali land; SP: swampland; BL: bare land; RG: rock and gravel; and AD: alpine desert.

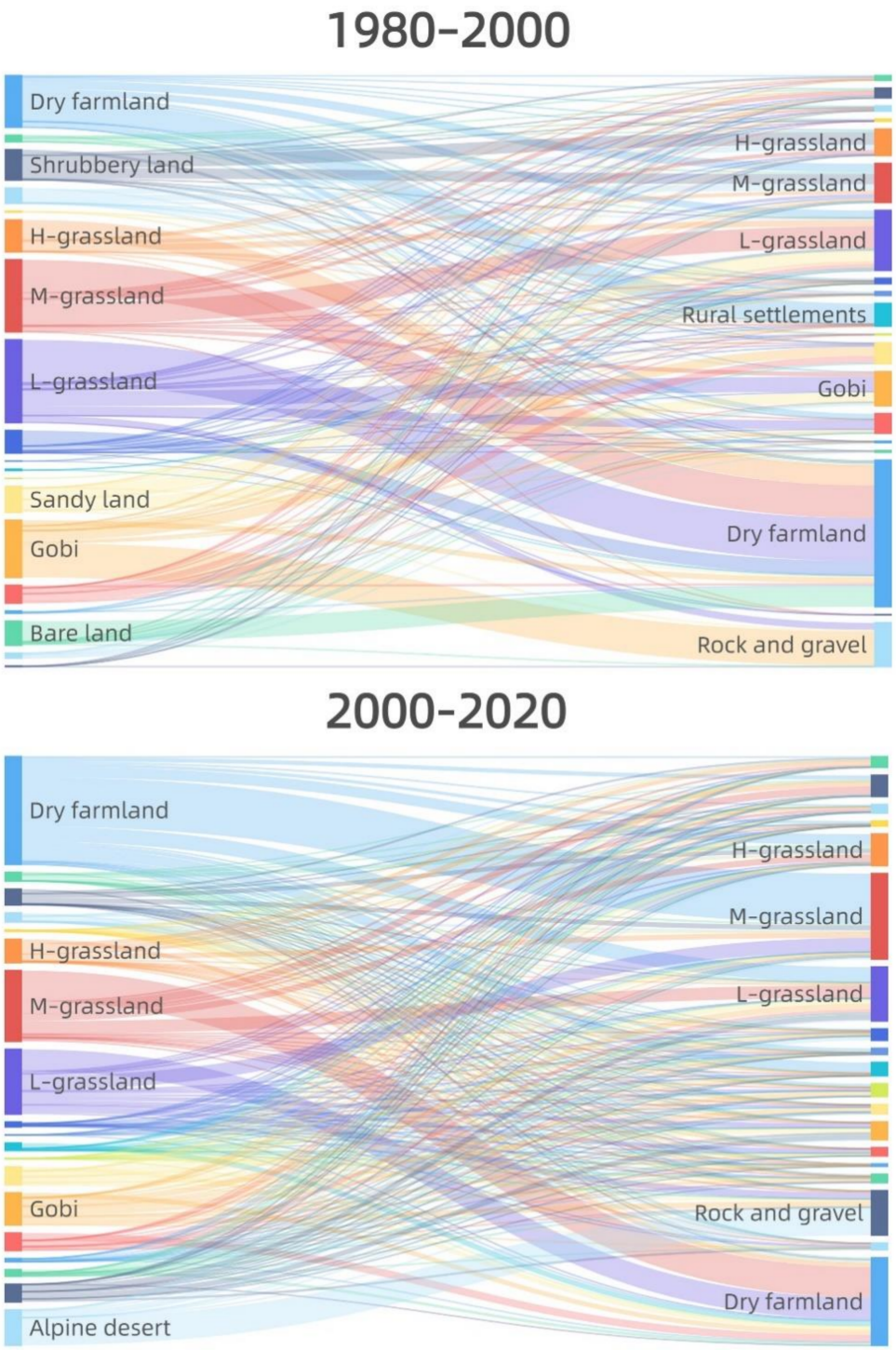

Figure 4. LUTC Sankey diagram of Gansu in 1980–2000 and 2000–2020.

3.2. Effects of LUCC on Carbon Storage during 1980–2020

Based on the InVEST model, the carbon storage of the Gansu province was estimated to reach 3393.2 ± 935.54 Tg C, 3290.54 ± 919.97 Tg C, and 3602.1 ± 1035.39 Tg C in 1980, 2000, and 2020, respectively (Tables 4 and S7), with a decrease from 1980 to 2000 (−3.03%), and an increase from 2000 to 2020 (9.47%). Furthermore, the CS of dry farmland, forest, and grassland reached 617.07 Tg C, 746.2 Tg C, and 1608.13 Tg C, respectively, accounting for about 86.66% of the total storage. Generally, the carbon storage of forestland, grassland, and unused land increased by time, while CS in dry farmland decreased.

Table 4. Carbon storage changes in the Gansu province from 1980 to 2020.

Top-Level Categories	Sub-Categories	Carbon Storage (Tg C)			
		1980	2000	2020	Change (1980–2020)
Farmland	Dry farmland	628.71	614.34	608.14	−20.57
Forest	Wood land	291.35	297.90	331.69	40.34
	Shrubbery land	311.22	312.67	347.28	36.06
	Sparsely forested woodland	98.85	101.13	117.60	18.75
	Other forest land	8.19	7.86	12.86	4.67
Grassland	High coverage grassland	534.33	500.54	535.06	0.73
	Middle coverage grassland	742.78	677.87	758.73	15.95
	Low coverage grassland	358.00	344.34	372.71	14.71
Water	River and glacier	0.00	0.00	0.00	0.00
Built-up land	Cities and towns	2.39	2.53	5.78	3.38
	Rural settlements	27.21	27.87	32.26	5.05
	Industry and traffic land	1.31	1.26	7.25	5.94
Unused land	Sandy land	50.85	54.40	64.91	14.06
	Gobi	131.55	132.18	149.18	17.63
	Saline-alkali land	28.95	27.84	24.55	−4.40
	Swampland	43.89	42.03	42.24	−1.65
	Bare land	13.05	12.00	13.76	0.71
	Rock and gravel	114.41	119.46	149.36	34.95
	Alpine desert	6.15	14.29	28.74	22.58

During 1980 to 2020, the spatial distribution of CS in the Gansu province was less varied (Figure 5a–c). Generally, regions with high values of CS were concentrated in Qilian Mountains and Gannan Plateau, where the precipitation favored the growth of forest and the temperature was low, enabling carbon accumulation in ecosystems. While the low values of CS were mainly distributed in Jiuquan city and the lower reaches of the Shiyang River Basin, where the main land-use type was dominated by Gobi, sandy, and other land-use types characterized by very low carbon density. In particular, the lower reaches of the Shiyang River Basin are surrounded by the Badain Jaran Desert and Tengger Desert, with strong solar radiation, low precipitation (<150 mm), and strong evaporation (2000–2600 mm), resulting in extremely sparse vegetation and low CS. It can be seen that the spatial distribution of CS in the Gansu province was closely related to the distribution of LUCC. The region dominated by forest and grassland has a high CS, while the region dominated by unused land, such as sandy, has a low CS. In 1980–2020, the CS in the Central Gansu province decreased significantly, while increased in western parts, and the alpine desert exhibited the most significant changes in carbon storage (Figure 5d).

To quantify the individual effect of LUTC on carbon storage changes, we assumed that the carbon density of each land-type was constant, and the difference between actual change and the land-use change-induced change can be regarded as the effects of other environmental drivers, such as climate change, CO_2 enrichment, and ecosystems managements. After estimations, the carbon storage of terrestrial ecosystem in the Gansu province increased by 208.9 ± 99.85 Tg C with a growth rate of 6.16% in 1980–2020, among which the increment in carbon storage bring by LUTC effect was 26.89 ± 5.81 Tg C (Table S8), thus the effect of multi-factor combination can reach to 182.01 ± 94.04 Tg C. Among them, the main land-use types with carbon storage decreases included two categories: degradation of high carbon density grassland and forest to low carbon density grassland (−17.06 Tg C) and reclamation of middle and high coverage grassland to dry farmland (−9.87 Tg C). Additionally, the LUTC that contributed to the increase in carbon storage included the reclamation of unused land into dry farmland (12.61 Tg C) and the restoration of dry farmland and low carbon density grassland to high carbon density grassland and forest (36.47 Tg C) (Figure 6).

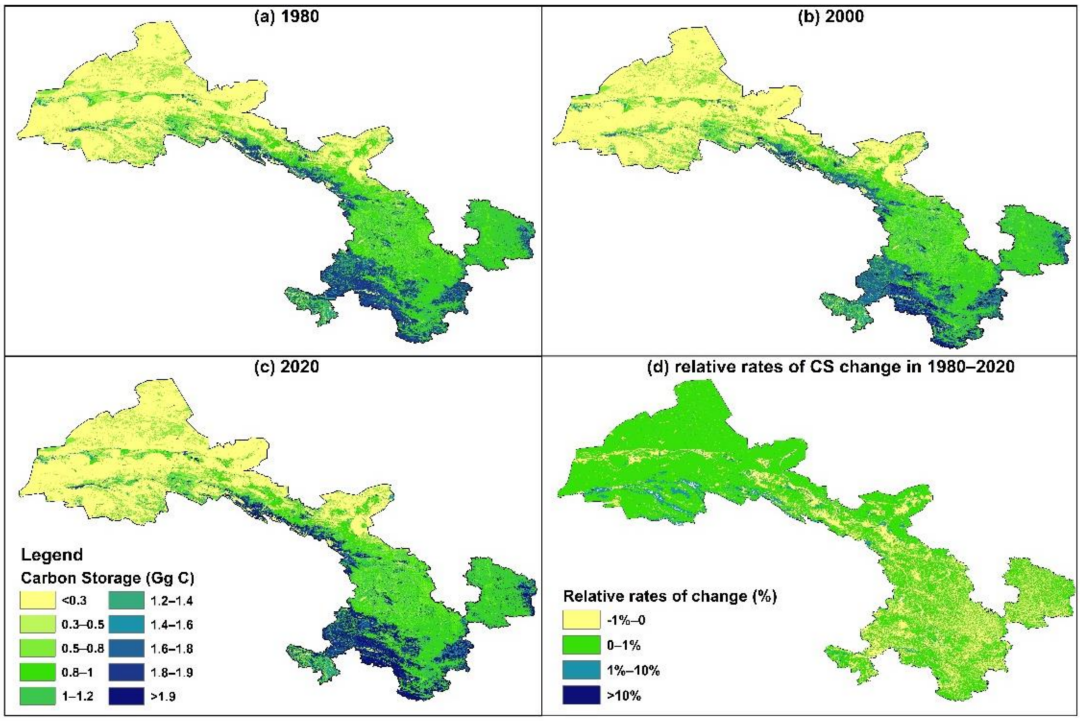

Figure 5. (**a**–**c**): The spatial distribution of CS across Gansu in 1980–2020; (**d**): The relative rates of CS change in 1980–2020. Note: Carbon storage per pixel (300 m × 300 m).

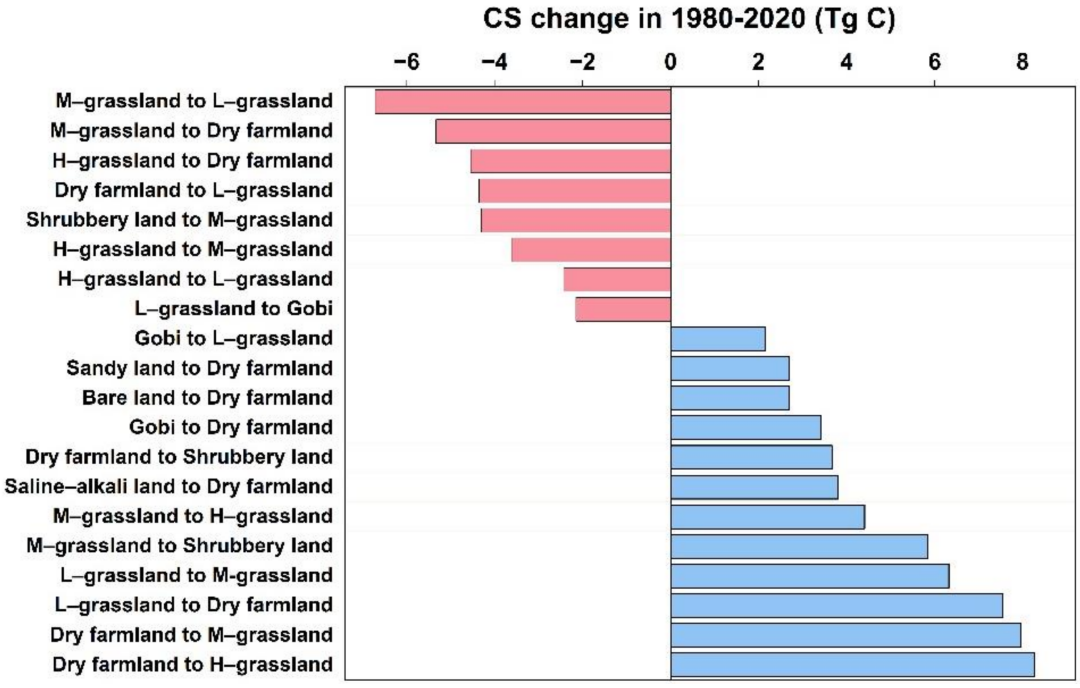

Figure 6. Carbon storage change in the Gansu province from 1980 to 2020.

3.3. Carbon Storage Changes under Different LUCC Scenarios

Under the NDS, the CS showed a decrease trend from 2020 to 2030, while the changes of CS in 2020–2050 were −14.69 ± 12.28 Tg C (−0.4%), 9.01 ± 29.12 Tg C (0.25%), and 57.83 ± 53.42 Tg C (1.6%) under the SSP126, SSP245, and SSP585, respectively. From 2020 to 2050, under EPS, the area of forests was supposed to increase by 13,409.19 km^2 (an increase of 34.83%), and the carbon storage was estimated to increase under all climate scenarios. This indicated that ecological protection projects (suitable afforestation in barren hills

and wasteland, protection and restoration of natural forest, and national forest reserves) were vital to the growth of forest area, leading to carbon storage increase (Figure S2; Tables 5, 6 and S9–S11).

Table 5. Area of LUCC in the Gansu province in 2030 and 2050 under the NDS and EPS scenarios.

LUCC	2020 (km^2)	NDS				EPS			
		2030 (km^2)	2020–2030 (%)	2050 (km^2)	2020–2050 (%)	2030 (km^2)	2020–2030 (%)	2050 (km^2)	2020–2050 (%)
Dry farmland	63,928.35	63,506.16	−0.66	68,885.19	7.75	55,827.81	−12.67	46,268.19	−27.62
Wood land	14,167.35	13,542.75	−4.41	13,468.86	−4.93	14,629.68	3.26	17,233.56	21.64
Shrubbery land	16,255.62	16,135.20	−0.74	15,940.62	−1.94	17,232.66	6.01	18,021.96	10.87
Sparsely forested woodland	7206.84	7342.29	1.88	7744.50	7.46	9420.30	30.71	10,658.34	47.89
Other forest land	874.35	787.32	−9.95	737.28	−15.68	3631.59	315.35	5999.49	586.17
High coverage grassland	26,488.44	25,344.72	−4.32	25,008.03	−5.59	25,763.76	−2.74	24,455.52	−7.67
Middle coverage grassland	60,983.10	63,719.01	4.49	60,708.87	−0.45	64,359.36	5.54	68,630.31	12.54
Low coverage grassland	56,115.72	58,050.99	3.45	65,219.85	16.22	58,320.36	3.93	63,200.43	12.63
River and glacier	3845.25	4280.31	11.31	4040.55	5.08	4424.67	15.07	5528.61	43.78
Cities and towns	904.77	1386.09	53.20	1729.35	91.14	1394.91	54.17	3052.26	237.35
Rural settlements	3443.40	3949.65	14.70	3910.14	13.55	3992.31	15.94	5810.13	68.73
Industry and traffic land	1241.28	3384.27	172.64	7718.31	521.80	3364.29	171.03	8127.36	554.76
Sandy land	28,120.41	27,747.27	−1.33	27,511.29	−2.17	27,773.37	−1.23	26,857.89	−4.49
Gobi	71,410.05	67,206.51	−5.89	58,971.15	−17.42	66,814.47	−6.44	58,547.97	−18.01
Saline-alkali land	7575.75	7534.44	−0.55	7289.91	−3.77	7323.39	−3.33	6841.35	−9.69
Swampland	2519.60	2426.58	−3.69	2534.76	0.60	2348.19	−6.80	2030.31	−19.42
Bare land	3892.14	4248.63	9.16	3699.54	−4.95	4166.91	7.06	4792.77	23.14
Rock and gravel	47,491.20	47,675.70	0.39	44,528.04	−6.24	47,593.08	0.21	44,971.11	−5.31
Alpine desert	8979.48	7152.12	−20.35	5773.77	−35.70	7038.90	−21.61	4392.45	−51.08

Table 6. Carbon storage changes in the Gansu province from 2020 to 2030 and from 2020 to 2050 under different LUTC Scenarios (NDS and EPS) and Future Climate Scenarios (SSP126, SSP245, and SSP585).

LUCC	2020 (Tg C)	NDS (Tg C)						EPS (Tg C)					
		SSP126		SSP245		SSP585		SSP126		SSP245		SSP585	
		2020–2030	2020–2050	2020–2030	2020–2050	2020–2030	2020–2050	2020–2030	2020–2050	2020–2030	2020–2050	2020–2030	2020–2050
Dry farmland	608.14	−6.19	47.90	−4.51	42.82	−6.65	36.68	−78.97	−167.50	−77.49	−170.91	−79.37	−175.03
Wood land	331.69	−14.29	−8.38	−13.38	−7.53	−13.83	−7.12	11.18	81.99	12.17	83.08	11.68	83.60
Shrubbery land	347.28	−4.00	−3.44	−2.85	−2.25	−3.30	−1.52	19.35	41.45	20.58	42.80	20.10	43.62
Sparsely forested woodland	117.60	2.85	14.72	3.27	14.34	2.96	14.56	36.94	64.51	37.47	63.99	37.08	64.28
Other forest land	12.86	−1.88	−3.14	−1.84	−3.34	−1.90	−3.49	37.81	66.25	37.95	64.60	37.70	63.39
High coverage grassland	535.06	−39.02	−65.84	−38.00	−66.93	−38.32	−63.87	−30.82	−76.21	−29.78	−77.28	−30.11	−74.28
Middle coverage grassland	758.73	12.92	−45.47	13.62	−53.57	13.36	−44.43	20.67	47.60	21.39	38.44	21.12	48.77
Low coverage grassland	372.71	10.58	53.22	12.24	59.81	12.95	73.15	12.36	40.03	14.03	46.42	14.74	59.35
River and glacier	0.00	0.00	0.00	0.00	0.00	0.00	0.00	0.00	0.00	0.00	0.00	0.00	0.00
Cities and towns	5.78	2.83	4.52	2.87	4.62	2.86	4.72	2.88	12.40	2.92	12.57	2.91	12.75
Rural settlements	32.26	3.06	0.52	3.19	0.37	3.06	0.06	3.45	16.45	3.57	16.22	3.44	15.77
Industry and traffic land	7.25	11.55	32.77	11.64	32.69	11.58	32.97	11.44	34.90	11.53	34.80	11.47	35.10
Sandy land	64.91	0.41	−0.19	1.24	4.61	1.70	9.13	0.47	−1.72	1.30	2.96	1.76	7.37
Gobi	149.18	−9.97	−31.47	−8.17	−23.19	−7.58	−16.57	−10.78	−32.31	−8.99	−24.09	−8.41	−17.52
Saline-alkali land	24.55	−1.52	−4.47	−1.20	−3.30	−1.21	−2.77	−2.16	−5.71	−1.85	−4.61	−1.87	−4.11
Swampland	42.24	−2.05	−1.23	−1.83	−0.10	−1.68	1.10	−3.34	−9.39	−3.13	−8.48	−2.99	−7.53
Bare land	13.76	0.94	−1.45	1.06	−1.08	1.07	−0.67	0.66	2.19	0.77	2.67	0.78	3.20
Rock and gravel	149.36	4.08	−5.82	5.98	5.45	7.18	15.91	3.82	−4.39	5.71	6.99	6.91	17.55
Alpine desert	28.74	1.52	2.56	1.61	5.59	2.47	10.00	1.04	−4.92	1.13	−2.62	1.98	0.73
Carbon Storage (Tg C)	3602.1	−28.17	−14.69	−15.06	9.02	−15.29	57.83	35.98	105.61	49.27	127.56	48.92	177.01

Under the NDS, the regions of carbon storage growth were mainly located in the oases of the Hexi Corridor under the SSP126 and SSP245 scenarios, while the southwestern Gansu was supposed to experience more carbon storage growth under the SSP585 scenario (Figure S3). In 2050, the carbon storage changes in the Gansu province were expected to increase in the west and decrease in the east under future climate scenarios. In particular, the Qilian Mountains and Gannan Plateau had abundant carbon storage and were highly sensitive to climate change. With the increase in temperature, soil carbon release will increase. Therefore, these regions were characterized by the most intense carbon lose. Under the EPS, the Hexi Corridor, Longnan, and Qingyang were the main regions characterized

by carbon storage growth, and the area of CS reduction was smaller than that under the NDS (Figure 7).

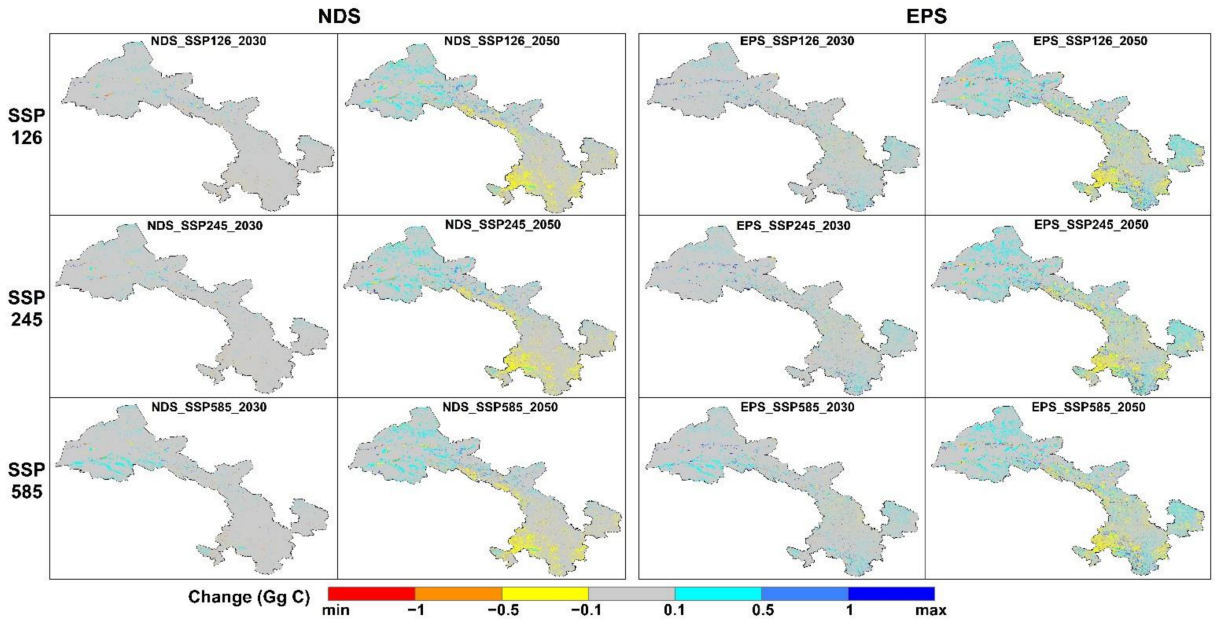

Figure 7. The spatial changes of the carbon storage across the Gansu province in the future periods (2030 and 2050) under the LUTC Scenarios (NDS and EPS) and Future Climate Scenarios (SSP126, SSP245, and SSP585) relative to 2020.

Under the NDS and EPS, AGC and BGC showed increasing trends with the rise of radiative forcing. SOC was negatively correlated with the temperature under the NDS, while the sequestration effect of SOC was enhanced as ecosystem management and restoration under the EPS. This was mainly associated with the effects of precipitation and CO_2 fertilization, which promoted vegetation growth under the high carbon emission and offset the negative effects of temperature on SOC [57,58]. Accordingly, the negative effect of SOC under NDS will decrease by 2050, and SOC under EPS will increase by 26.98 Tg C (Figure 8).

Based on the assumption that land type carbon density was constant, the individual effect of LUTC on carbon storage in terrestrial ecosystems was revealed for future three decades. In 2020–2050, the carbon storage was estimated to increase by 56.46 ± 9.82 Tg C (1.67%) and 165.84 ± 40.06 Tg C (4.9%) as results of LUTC effects under the NDS and EPS, respectively (Figure 9). Under the scenario of NDS, the main cause of future carbon storage reduction was the degradation of grasslands (−20.39 Tg C), and the main type of conversion that caused carbon storage growth was the governance of unused land (e.g., conversion of Gobi to low coverage grassland and dry farmland) (62.83 Tg C). Under the EPS, the conversion land types that caused the decline in carbon storage were the degradation of high coverage grassland to middle coverage grassland (−12.01 Tg C) and the conversion of dry farmland to low coverage grassland, as well as cities and towns (−13.43 Tg C). The LUTC for carbon storage growth mainly originated from ecological management restoration. Except for the planned and management of unused land (58.25 Tg C), the ecological restoration of dry farmland and low carbon density grassland to high carbon density grassland and forest (110.26 Tg C) totally accounted for 65.43% of the carbon increment from 2020 to 2050 under EPS.

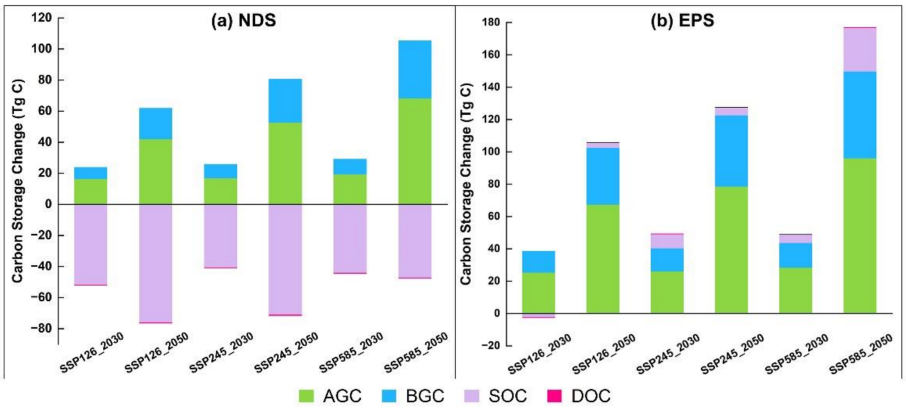

Figure 8. The change in the carbon storage of AGC, BGC, SOC, and DOC across the Gansu province in the future periods (2030 and 2050) and Future Climate Scenarios (SSP126, SSP245 and SSP585) relative to 2020. (**a**) NDS and (**b**) EPS are the different LUTC Scenarios.

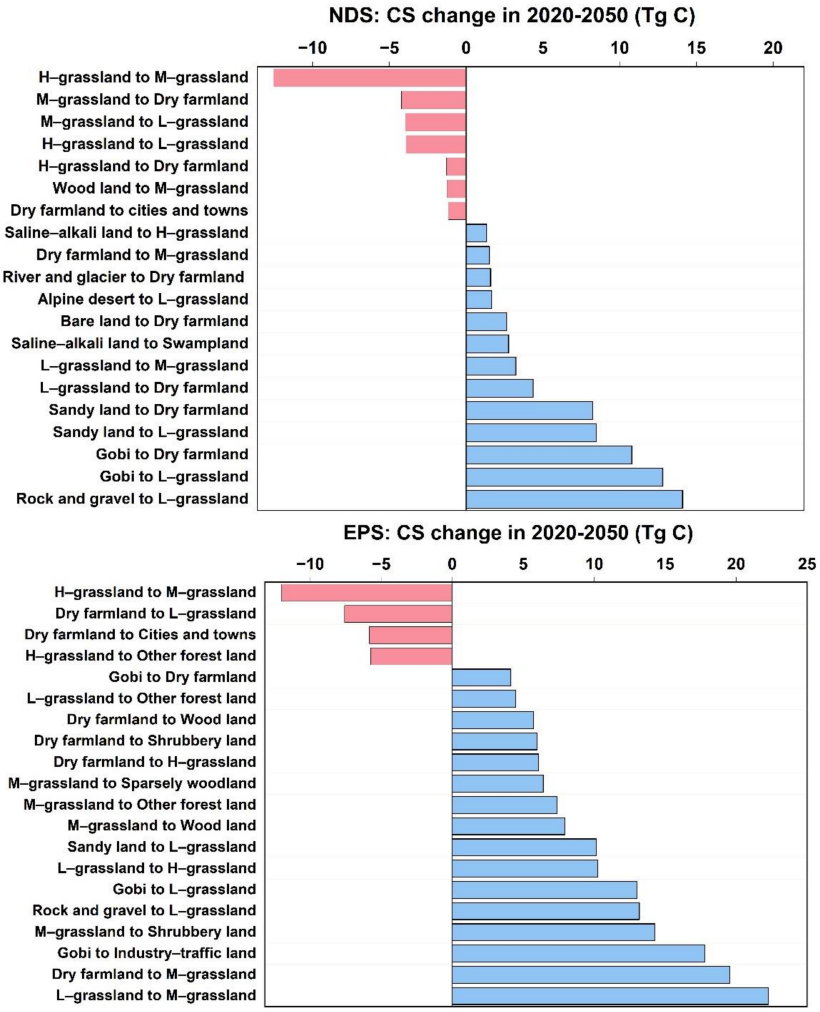

Figure 9. The major LUTC for CS change under NDS and EPS scenarios from 2020 to 2050 in the Gansu province.

4. Discussion

4.1. Terrestrial Ecosystem Carbon Storage in the Gansu Province

Based on the high-resolution standard carbon density dataset derived from remote sensing indexes and machine learning algorithms, we quantified the high-precision vegetation and soil carbon density data of 19 land-use types in the Gansu province, and our

results are similar with those obtained from field measurements. For example, the average soil carbon density of the Gansu province calculated in this study was 7.53 kg C m^{-2}, which was close to the results of Liu et al. [63] with a soil carbon density of 0–100 cm in the Loess Plateau of 7.70 kg C m^{-2}. Although high-precision carbon density data were used to estimate carbon storage with the InVEST model, carbon density might fluctuate due to the influence of carbon deposition, climate change, and other factors, leading to uncertainty for carbon storage change estimation over time. Therefore, this study also considered the effects of these factors on vegetation, soil, and dead organic carbon to obtain the carbon density dynamics of AGC, BGC, SOC, and DOC for different periods in the Gansu province. These high-precision carbon density datasets and the carbon density dynamics should be considered in future carbon storage calculation by the InVEST model, which can better reflect the variability of the spatial and temporal distribution of carbon density with more regional characteristics, rather than just based on literature statistics.

Before integrating the MCE-CA-Markov model and InVEST model to predict the evolution trends of land use and carbon storage of the Gansu province in 2030 and 2050 under the NDS and EPS scenarios, the simulation results were validated with 10-year and a 20-year cycles. The kappa coefficients were all greater than 0.9 and FoM coefficients were 0.25. Considering the large area, complex climatic conditions, and significant regional differences, the simulation accuracy is satisfactory, indicating that MCE-CA-Markov can capture the spatial evolution characteristics of each land-use type in the Gansu province. Wang et al. [19] concluded that the CA-Markov and FLUS models had better simulation results in the arid region after comparing multiple land-use prediction models. Ashraf et al. [64] also used the CA-Markov model to validate the LUCC simulation in the arid zone of Pakistan. In this study, we used dynamic carbon density data to estimate the actual changes in carbon storage, while using time-static carbon density data to determine the individual impact of land-use change on carbon storage. The results enabled us to better understand the influencing role of LUCC in the changes in carbon, and provide guidance for future land-use management and the designation of carbon emission reduction measures.

4.2. Effect of LUCC on CS during 1980–2020

From 1980 to 2020, the carbon storage of terrestrial ecosystem in the Gansu province increased by 208.9 ± 99.85 Tg C, of which the increment in carbon storage brought by the LUTC effect was 26.89 ± 5.81 Tg C. Therefore, the contribution of other elements to carbon storage change could reach 182.01 ± 94.04 Tg C. Except for land-use elements, this study also discussed the effects of temperature, precipitation, CO_2 fertilization effects, and the management of forest and agriculture on carbon storage changes. Firstly, the spatial pattern distribution of carbon density in terrestrial ecosystems was significantly correlated with climate (Tables S1 and S2), showing a negative correlation with temperature and positive correlation with precipitation, which was consistent with the findings of Tang et al. [65]. From 2000 to 2020, the change in average annual precipitation in the Gansu province was 41.65 mm, which was much higher than that of 1980–2000 (−13.72 mm). The significant increase in precipitation promoted the growth of vegetation, which increased SOC and promoted the growth in carbon storage in the terrestrial ecosystem. During the past 40 years, the Gansu province warmed by 1.33 °C. Referring to the study of [66], the increased temperature enriched the input of organic matter to soil by increasing vegetation productivity and then influenced the input and loss of SOC through enhanced microbial activity to decompose organic matter in the presence of sufficient soil moisture. An increase in CO_2 concentration could increase biomass by promoting plant growth, which in turn increased the dead organic matter returned to the soil, thus promoting carbon input to soil and causing the accumulate of SOC. The transition from young growth forest to overmature forest improved the forest carbon sequestration capacity, contributing to the growth in carbon storage [67]. Agricultural management (e.g., straw/stover return to soils) could increase agricultural soil carbon sequestration by charring straw into biomass char for application to agricultural fields [68].

There were four main reasons for the carbon storage growth caused by the LUTC effect: natural forest protection and restoration, grassland protection and restoration, the grain for green on the Loess Plateau, and agricultural development in the Hexi Corridor (Figures 5d and 6). In the Qilian Mountains and the Gannan Plateau, the conversion of middle and high coverage grasslands to forest increased the above-ground biomass, the amount of plant residues of soil, and the content of the topsoil organic matter, which increased the carbon storage of the forest ecosystem. The imbalance between grassland and livestock in the Gansu province was quite serious over the last century, with overgrazing leading to grassland degradation. However, after the implementation of forage-livestock balance, and ecological management and restoration, low-carbon-density grasslands were transformed into high-carbon-density grasslands. Different from forest ecosystems, the carbon pools of grassland ecosystems were mainly concentrated in the subsurface and stored in the soil and plant roots so that the soil organic carbon storage increased with the governance of grassland, and significantly enhanced the carbon sink of grassland ecosystems.

The implementation of the grain for green promoted the growth of carbon storage in the Loess Plateau, meanwhile the agricultural development in the Hexi Corridor also contributed to the growth of carbon storage (Figure 5d). Regional differences were the reason why the transfer into and out of dry farmland promotes the growth in carbon storage. The Loess Plateau was richer in precipitation and more suitable for vegetation growth, so the carbon density of natural vegetation was higher. However, the conversion of natural vegetation to dry farmland destroyed the underground biomass and the carbon sink capacity of soil organic matter. Since the implementation of the grain for green projects, the dry farmland was restored to natural vegetation, and the carbon stock was increased due to enhanced biomass input into soils. In arid desertification areas, the natural desert soil was rich in sand particles and had a loose structure with very low organic carbon and nutrient contents. After being reclaimed for cultivation, management measures such as irrigation, fertilization, and tillage significantly increased the input of biomass, root carbon as well as other organic substances, so that the carbon storage of the ecosystem showed an increasing trend, which was similar to the results of previous studies [69].

4.3. Carbon Storage Changes under Different LUCC Scenarios

If we only consider the effects of LUTC, the carbon storage in 2050 was estimated to reach 3440.08 ± 968.48 Tg C and 3549.46 ± 998.72 Tg C under the NDS and EPS, with an increase of 56.24 ± 9.82 Tg C (1.63%) and 165.26 ± 40.06 Tg C (4.66%) in comparison with 2020, respectively (Table S11). If we additionally consider the effects of other environmental drivers, the carbon storage in 2030 (SSP126, SSP245, and SSP585) and 2050 (SSP126) under NDS was lower than that in 2020. We deduced that this was mainly associated the climate warming, which strengthened the water pressure and accelerated soil carbon decomposition rates, leading to lower carbon storage. From 2020 to 2050, the average precipitation increment in the Gansu province was small, but the temperature increase was much significant, which may cause the loss of SOC. Compared with SSP126 and SSP245, the CO_2 concentration increases significantly under SSP585, which played a fundamental role in the carbon storage growth in terrestrial ecosystem.

Moreover, under the same climate change scenario, carbon storage was higher under EPS than that under NDS (Figure 10), indicating that terrestrial ecosystems have great potential for carbon sequestration, especially based on the optimization of existing land resources management. Therefore, the optimal management of land resources to increase carbon storage should be a key concern of the government. At present, documents such as the 14th Five-Year Plan for National Economic and Social Development of Gansu province and the Outline of long-term Goals in 2035 pointed out that the Gansu province should carry out a new-style urbanization construction under the premise of ecological protection, which showed that the expansion of urban areas may occupy part of the cultivated land. In addition, the future population concentration and urbanization will be more significant than at present. Thus, the protection, restoration, and increase in high carbon density

forests and grasslands, where possible, may be the inevitable way to achieve carbon peak and carbon neutrality in China, which was also discussed in other research [29,70].

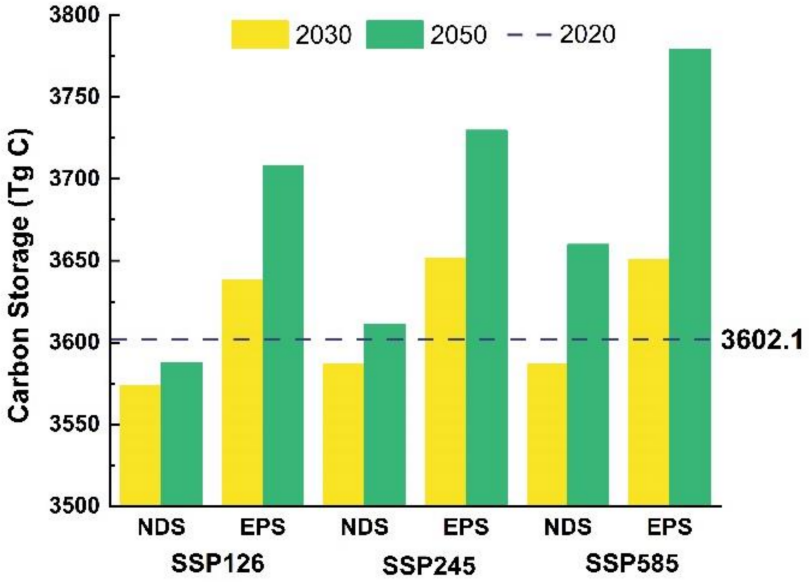

Figure 10. The carbon storage in the future periods (2030 and 2050) under the LUTC Scenarios (NDS and EPS) and Future Climate Scenarios (SSP126, SSP245 and SSP585) in Gansu province.

Under the two scenarios, regions with decreasing carbon storage were mainly distributed in the southern part of Jiuquan, while regions with increasing carbon storage were mostly located in the oases of the Hexi Corridor and the north-central part of Jiuquan. Additionally, compared with NDS, the CS in the Qilian Mountains and Gannan Plateau was expected to increase under the EPS. The increase in CS in central and northern part of Jiuquan was mainly due to the conversion of unused land to low coverage grassland, while the decrease in CS in the southern part was mainly because of the transfer of other unused land to rock and gravel. Under the NDS, the conversion of unused land to dry farmland and low coverage grassland in the Hexi Corridor will increase CS. Under EPS, in addition to the conversion of unused land to low coverage grassland, the restoration of forests in the Qilian Mountains and Gannan Plateau will also contribute to the increase in CS.

At present, there is still some distance from the goal of carbon peak and carbon neutrality. In the contemporary era of new-style urbanization, we cannot reduce carbon emissions at the expense of economic development. Therefore, carbon sequestration measures based on ecological protection perspective are the main initiatives to be taken. Because of the early damage of forest and grassland ecosystems in the Gansu province, the carbon accumulated in vegetation and soil is lower. However, with the promotion and implementation of ecological restoration projects, there is a strong potential for carbon sequestration in the future, especially in the deep soil layer. Therefore, reasonable ecological restoration measures to enhance carbon storage of terrestrial ecosystems remain important steps to mitigate the increase in atmospheric CO_2 concentration and improve the environment.

4.4. Implications for Carbon Management

In future, although the rise of temperature will bring negative effect to the increase in ecosystem carbon storage, the vegetation growth recovery, CO_2 fertilization effect, and the management of forest and agriculture could offset the negative effect of temperature to some extent. Therefore, the future carbon sequestration capacity of terrestrial ecosystem mainly depends on the areas of ecological restoration. Due to the long and narrow geographical area of the Gansu province, the landscapes varied tremendously over space, so it is necessary to develop targeted initiatives according to local conditions and issues. In the Loess Plateau, precipitation is richer, while the soil is porous and easy to erode. It

is necessary to keep carrying forward the project of grain for green to return dry farmland to forest and grass in areas unsuitable for cultivation and need protection, such as dry farmland with a slope of 25 degrees or more, sandy farmland, and important water reserves. In addition, climate and environmental factors should be taken into account in assessing the suitability of returning forests or grassland to prevent soil drought, which is not only detrimental to the restoration of forests and grasses, but also reduces the stability of the ecosystem.

In the Hexi Corridor, the issue of carbon storage is ultimately a matter of water resources availability [40]. Precipitation in the Hexi Corridor is scarce, and the runoff of the inland river basins (the Shule River, Heihe River, and Shiyang River) is limited, making it difficult to supply the growth of extensive forest and grasslands. Especially, the growth of forest requires a large amount of water resources. If the water supply cannot sustain the vegetation development, it may endanger the safety of groundwater quantity and lead to rapid degradation of the ecosystem, which in turn lead to the return of carbon fixed in vegetation and soil to the atmosphere. Therefore, apart from effectively utilizing water resources, it is also necessary to reasonably increase the amount of ecological water consumption to improve the regional ecological environment and increase carbon sequestration capacity.

For the Qilian Mountains and Gannan Plateau, we should focus on the protection and restoration of forest and grassland to improve vegetation cover, and thus increasing carbon sequestration capacity. In addition, with the influence of climate warming, the melting of permafrost in alpine mountainous regions could cause the decomposition of organic matter, which may release large amounts of carbon [71]. Li et al. [40] also suggested that, in alpine regions, warming will accelerate the release rate of soil carbon, thus effective measures, such as planting zonal shrub species to increase the coverage, should be taken into practice to reduce the surface temperature.

4.5. Limitations and Uncertainties

There are some limitations as well as uncertainties in this study. First, although we considered the effects of temperature, precipitation, CO_2 fertilization, and managements of forest and agricultural lands in estimating carbon density dynamics for each period (Tables S3–S6), there may be some factors that we overlooked, such as the effects of natural disasters as wildfires, floods, and droughts [72]. Based on global fire statistics, Shi et al. concluded that total carbon emissions from forest fires increased by 26% in 2019 compared to the previous year and believe that persistent fire events may alter vegetation composition, leading to the reduction in carbon storage in terrestrial ecosystems [73]. However, based on statistical yearbook, we counted forest fires in the Gansu province from 2000–2017 (Table S12) and concluded that the number of fires and the total burning area in the Gansu province is quite small, and the area of affected forests was even smaller. Moreover, the source of most fires was related to human activities, with fewer fire events related to climate warming. Therefore, we believe that the effect of fire on carbon storage needs to be considered at the global scale and region with frequent fires events, but the effect of fire on carbon storage in regions with less forest fire can be negligible.

Secondly, in this study, the multiple linear regression between climate data (precipitation and temperature) and above- and below-ground biomass carbon density were derived from historical climate data and standard carbon density data, and then the carbon densities of the four major carbon pools in different periods were measured by combining temperature and precipitation data in the corresponding periods. Three Global Climate Models (EC-Earth3, GFDL-ESM4, and MRI-ESM2-0) were used for ensemble averaging when predicting future carbon density data under different scenarios. Although ensemble averaging could minimize the uncertainties of single climate models, climate prediction inevitably had certain uncertainties.

In addition, this study set up two development scenarios of natural development and ecological protection based on the social development pattern. The MCE-CA-Markov

model can reflect the spatial distribution of land-use changes under different scenarios (Figure S2). However, it was difficult to accurately quantify and assess the effects of temperature and precipitation on land types in the process of producing the suitability atlas on each land type, and the future development patterns of special areas, such as national forest parks and nature reserves, were not considered separately, which may lead to uncertainty in future land-use simulations. By introducing deep learning algorithms to explain the spatial relationship characteristics of geography, climate, social development, and other elements with the land types, we can portray their intrinsic information more richly, which is the direction of further research and optimization.

5. Conclusions

Based on the land-use and standard high-resolution carbon density data of 19 land use types in the Gansu province from 1980 to 2020, this study integrated temperature, precipitation, CO_2 fertilization effect, and forest agriculture management to establish the tables of carbon density dynamic data and simulated the spatial distribution of LUCC in 2030 and 2050 under NDS and EPS by MCE-CA-Markov. After that, two types of effect (only LUTC effect and multi-factor combination effect) were used to assess the spatial and temporal evolution of the carbon storage of historical and future periods. The main conclusions are as follows:

(1) Throughout 1980–2020, the land-use type of Gansu was dominated by Gobi, dry farmland, middle coverage grassland, low coverage grassland, and rock and gravel. Additionally, the area changes of forests, grasslands, water, and constructions were rising, while dry farmland and unused land showed a trend of decreasing. Besides, LUTC in 2000–2020 has been more dramatic. The largest area of conversion types in the southeastern Gansu was middle coverage grassland, low coverage grassland, and dry farmland, while the northwestern part was dominated by the interconversion of rock and gravel, Gobi, and low coverage grassland.

(2) The carbon storage of terrestrial ecosystem in the Gansu province increased by 208.9 $\pm$ 99.85 Tg C with a growth rate of 6.16% from 1980 to 2020. Among this, the LUTC effect contributed 26.89 $\pm$ 5.81 Tg C, and other environmental controls together contributed to another 182.01 $\pm$ 94.04 Tg C. As for the LUTC effect, the restoration of dry farmland and low carbon density grassland to high carbon density grassland and forest (36.47 Tg C) and degradation of high carbon density grassland and forest to low carbon density grassland ($-$17.06 Tg C) were the main components of carbon storage changes. The CS in Central Gansu decreased significantly, while that in western Gansu increased, and the alpine desert showed the most significant changes in carbon storage.

(3) Under the NDS, carbon storage was expected to exhibit a decrease trend during 2020–2030, while the changes in carbon storage from 2020 to 2050 were $-$14.69 $\pm$ 12.28 Tg C ($-$0.4%), 9.01 $\pm$ 29.12 Tg C (0.25%), and 57.83 $\pm$ 53.42 Tg C (1.6%) under the SSP126, SSP245, and SSP585 scenarios, respectively. Under the EPS, the carbon storage corresponding to the future climate scenarios all showed an increasing trend. The LUTC effects were predicted to increase ecosystem carbon storage by 56.46 $\pm$ 9.82 Tg C (1.67%) and 165.84 $\pm$ 40.06 Tg C (4.9%) under the NDS and EPS from 2020 to 2050, and the management of unused land was the main reason for the growth of carbon storage. Therefore, future carbon sequestration capacity of terrestrial ecosystem may mainly depend on ecological restoration efforts.

Supplementary Materials: The following supporting information can be downloaded at: https://www.mdpi.com/article/10.3390/rs14133164/s1, Figure S1: The spatial distribution of uncertainty (expressed as standard error) for each carbon density; Figure S2: Spatial distribution of LUCC of 2030 and 2050 in Gansu under NDS and EPS; Figure S3: Spatial distribution of CS in 2030 and 2050 in Gansu under LUCC Scenarios (NDS and EPS) and Future Climate Scenarios (SSP126, SSP245 and SSP585); Table S1: The coefficients of multiple linear regression equations for both above- and below-

ground biomass carbon density as dependent variable of temperature and precipitation; Table S2: The coefficients of multiple linear regression equations for soil carbon density as dependent variable of precipitation, temperature, above- and below-ground biomass carbon density, temperature, and precipitation; Table S3: The AGC density of different land types from 1980 to 2050; Table S4: The BGC density of different land types from 1980 to 2050; Table S5: The SOC density of different land types from 1980 to 2050; Table S6: The DOC density of different land types from 1980 to 2050; Table S7: The CS of each land type in Gansu Province from 1980 to 2020; Table S8: The CS from 1980 to 2020 under only LUTC effect; Table S9: The CS of each land type in Gansu Province of 2030 and 2050 with Future Climate Scenarios (SSP126, SSP245, and SSP585) under NDS; Table S10: The CS of each land type in Gansu Province of 2030 and 2050 with Future Climate Scenarios (SSP126, SSP245, and SSP585) under EPS; Table S11: The CS of 2030 and 2050 under only LUTC effect; Table S12: Fire statistics of Gansu Province from 2000 to 2017.

Author Contributions: Conceptualization, L.W., R.Z. and Z.Y.; methodology, L.W., Z.Y., R.Z. and Z.C.; validation, L.W. and Z.Y.; formal analysis, L.W.; resources, L.W. and Z.Y.; data curation, R.L. and C.F.; writing—original draft preparation, L.W.; writing—review and editing, R.Z., Z.Y. and Z.C.; supervision, Z.Y. and R.Z.; project administration, Z.Y. and R.Z.; funding acquisition, R.Z., Z.Y., J.Z. and Y.F. All authors have read and agreed to the published version of the manuscript.

Funding: This research was funded by the National Natural Science Foundation of China (42161018, 52179026), Youth Innovation Promotion Association CAS, Science and technology project of the Gansu province (21ZD4NF044-02), the XPCC Science and Technique Foundation (2021AB021), and Opening Fund of the Technology Innovation Center for Mine Geological Environment Rehabilitation Engineering in Alpine and Arid Regions, Ministry of Natural Resources (HHGGKK2102), the Gansu Science and Technology Association Youth Science and Technology Talent Support Project (GXH20210611-09).

Acknowledgments: The authors would like to thank the editors and anonymous reviewers for their detailed and constructive comments, which helped to significantly improve the manuscript.

Conflicts of Interest: The authors declare no conflict of interest.

References

1. IPCC. *Climate Change 2014: Synthesis Report*; Contribution of Working Groups I, II and III to the Fifth Assessment Report of the Intergovernmental Panel on Climate Change; World Meteorological Organization: Geneva, Switzerland, 2014; 151p.
2. Chacko, S.; Ravichandran, C.; Vairavel, S.M.; Mathew, J. Employing Measurers of Spatial Distribution of Carbon Storage in Periyar Tiger Reserve, Southern Western Ghats, India. *J. Geovis. Spat. Anal.* **2019**, *3*, 1. [CrossRef]
3. Pang, J.X.; Li, H.J.; Lu, C.P.; Lu, C.Y.; Chen, X.P. Regional Differences and Dynamic Evolution of Carbon Emission Intensity of Agriculture Production in China. *Int. J. Environ. Res. Public Health* **2020**, *17*, 7541. [CrossRef] [PubMed]
4. United Nations (UN). "Today Is an Historic Day", Says Ban, as 175 Countries Sign Paris Climate Accord. UN News 2016. Available online: https://news.un.org/en/story/2016/04/527442-today-historic-day-says-ban-175-countries-sign-paris-climate-accord (accessed on 18 October 2021).
5. Jiang, K.J.; Tamura, K.; Hanaoka, T. Can we go beyond INDCs: Analysis of a future mitigation possibility in China, Japan, EU and the U.S. *Adv. Clim. Change Res.* **2017**, *8*, 117–122. [CrossRef]
6. Wang, H.K.; Lu, X.; Deng, Y.; Sun, Y.G.; Nielsen, C.P.; Liu, Y.F.; Zhu, G.; Bu, M.L.; Bi, J.; McElroy, M.B. China's CO_2 peak before 2030 implied from characteristics and growth of cities. *Nat. Sustain.* **2019**, *2*, 748–754. [CrossRef]
7. IPCC. *IPCC Special Report on Global Warming of 1.5 °C Geneva*; World Meteorological Organization: Geneva, Switzerland, 2018; Available online: https://www.ipcc.ch/sr15/ (accessed on 18 October 2021).
8. Zou, C.N.; Xiong, B.; Xue, H.Q.; Zheng, D.W.; Ge, Z.X.; Wang, Y.; Jiang, L.Y.; Pan, S.Q.; Wu, S.T. The role of new energy in carbon neutral. *Petrol. Explor. Dev.* **2021**, *48*, 480–491. [CrossRef]
9. Xia, C.Y. *Multi-Scale Studies on Urban Carbon Metabolism from the Perspective of Land Use and Scenario Analysis of Emission Reduction*; Zhejiang University: Hangzhou, China, 2019. [CrossRef]
10. Wang, Z.Y.; Li, X.; Mao, Y.T.; Li, L.; Wang, X.R.; Lin, Q. Dynamic simulation of land use change and assessment of carbon storage based on climate change scenarios at the city level: A case study of Bortala, China. *Ecol. Indic.* **2022**, *134*, 108499. [CrossRef]
11. Xiong, C.H.; Wang, G.L.; Xu, L.T. Spatial differentiation identification of influencing factors of agricultural carbon productivity at city level in Taihu lake basin, China. *Sci. Total. Environ.* **2021**, *800*, 149610. [CrossRef]
12. Chen, B.Y.; Xu, C.; Wu, Y.Y.; Li, Z.W.; Song, M.L.; Shen, Z.Y. Spatiotemporal carbon emissions across the spectrum of Chinese cities: Insights from socioeconomic characteristics and ecological capacity. *J. Environ. Manag.* **2022**, *306*, 114510. [CrossRef]
13. Gonçalves, D.R.P.; Mishra, U.; Wills, S.; Gautam, S. Regional environmental controllers influence continental scale soil carbon stocks and future carbon dynamics. *Sci. Rep.* **2021**, *11*, 6474. [CrossRef]

14. Janes-Bassett, V.; Bassett, R.; Rowe, E.C.; Tipping, E.; Yumashev, D.; Davies, J. Changes in carbon storage since the pre-industrial era: A national scale analysis. *Anthropocene* **2021**, *34*, 100289. [CrossRef]
15. Zhou, R.B.; Lin, M.Z.; Gong, J.Z.; Wu, Z. Spatiotemporal heterogeneity and influencing mechanism of ecosystem services in the Pearl River Delta from the perspective of LUCC. *J. Geogr. Sci.* **2019**, *29*, 831–845. [CrossRef]
16. Adelisardou, F.; Jafari, H.; Malekmohammadi, B.; Minkina, T.; Zhao, W.W.; Karbassi, A. Impacts of land use and land cover change on the interactions among multiple soil-dependent ecosystem services (case study: Jiroft plain, Iran). *Environ. Geochem. Health* **2021**, *43*, 11. [CrossRef]
17. Li, X.D.; Ling, F.; Giles, F.; Du, Y. A superresolution land-cover change detection method using remotely sensed images with different spatial resolutions. *IEEE Trans. Geosci. Remote Sens.* **2016**, *54*, 3822–3841. [CrossRef]
18. Tong, J.H.; Hu, J.H.; Lu, Z.; Sun, H.R.; Yang, X.F. The impact of land use and cover change on soil organic carbon and total nitrogen storage in the Heihe River Basin: A meta-analysis. *J. Geogr. Sci.* **2019**, *29*, 1578–1594. [CrossRef]
19. Wang, Q.Z.; Guan, Q.Y.; Lin, J.K.; Luo, H.P.; Tan, Z.; Ma, Y.R. Simulating land use/ land cover change in an arid region with the coupling models. *Ecol. Indic.* **2021**, *122*, 107231. [CrossRef]
20. Zhu, G.F.; Qiu, D.D.; Zhang, Z.X.; Sang, L.Y.; Liu, Y.W.; Wang, L.; Zhao, K.L.; Ma, H.Y.; Xu, Y.X.; Wan, Q.Z. Land-use changes lead to a decrease in carbon storage in arid region, China. *Ecol. Indic.* **2021**, *127*, 107770. [CrossRef]
21. Leh, M.D.K.; Matlock, M.D.; Cummings, E.C.; Nalley, L.L. Quantifying and mapping multiple ecosystem services change in West Africa. *Agric. Ecosyst. Environ.* **2013**, *165*, 6–18. [CrossRef]
22. Dargains, A.; Cabral, P. A GIS-based methodology for sustainable farming planning: Assessment of land use/cover changes and carbon dynamics at farm level. *Land Use Policy* **2021**, *111*, 105788. [CrossRef]
23. Araya, Y.H.; Cabral, P. Analysis and Modeling of Urban Land Cover Change in Setúbal and Sesimbra, Portugal. *Remote Sens.* **2010**, *2*, 1549. [CrossRef]
24. Azizi, A.; Malakmohamadi, B.; Jafari, H.R. Land use and land cover spatiotemporal dynamic pattern and predicting changes using integrated CA-Markov model. *Glob. J. Enviro. Sci. Manag.* **2016**, *2*, 223–234. [CrossRef]
25. Chen, G.Z.; Li, X.; Liu, X.P.; Chen, Y.M.; Liang, X.; Leng, J.Y.; Xu, X.C.; Liao, W.L.; Qiu, Y.A.; Wu, Q.L.; et al. Global projections of future urban land expansion under shared socioeconomic pathways. *Nat. Commun.* **2020**, *11*, 537. [CrossRef] [PubMed]
26. Jiang, X.W.; Bai, J.J. Predicting and assessing changes in NPP based on multi-scenario land use and cover simulations on the Loess Plateau. *J. Geogr. Sci.* **2021**, *31*, 977–996. [CrossRef]
27. Raji, S.A.; Odunuga, S.; Fasona, M. Spatially Explicit Scenario Analysis of Habitat Quality in a Tropical Semi-arid Zone: Case Study of the Sokoto–Rima Basin. *J. Geovis. Spat. Anal.* **2022**, *6*, 11. [CrossRef]
28. Liang, X.; Guan, Q.F.; Clarke, K.C.; Liu, S.S.; Wang, B.Y.; Yao, Y. Understanding the drivers of sustainable land expansion using a patch-generating land use simulation (PLUS) model: A case study in Wuhan, China. *Comput. Environ. Urban.* **2021**, *85*, 101569. [CrossRef]
29. Li, C.; Wu, Y.M.; Gao, B.P.; Zheng, K.J.; Wu, Y.; Li, C. Multi-scenario simulation of ecosystem service value for optimization of land use in the Sichuan-Yunnan ecological barrier, China. *Ecol. Indic.* **2021**, *132*, 108328. [CrossRef]
30. Xu, J.R.; Renaud, F.G.; Barrett, B. Modelling land system evolution and dynamics of terrestrial carbon stocks in the Luanhe River Basin, China: A scenario analysis of trade-offs and synergies between sustainable development goals. *Sustain. Sci.* **2021**. [CrossRef] [PubMed]
31. Trisurat, Y.; Eawpanich, P.; Kalliola, R. Integrating land use and climate change scenarios and models into assessment of forested watershed services in Southern Thailand. *Environ. Res.* **2016**, *147*, 611–620. [CrossRef]
32. Jiang, W.G.; Deng, Y.; Tang, Z.H.; Lei, X.; Chen, Z. Modelling the potential impacts of urban ecosystem changes on carbon storage under different scenarios by linking the CLUE-S and the InVEST models. *Ecol. Model.* **2017**, *345*, 30–40. [CrossRef]
33. Matlhodi, B.; Kenabatho, P.K.; Parida, B.P.; Maphanyane, J.G. Analysis of the Future Land Use Land Cover Changes in the Gaborone Dam Catchment Using CA-Markov Model: Implications on Water Resources. *Remote Sens.* **2021**, *13*, 2427. [CrossRef]
34. Mokarram, M.; Pourghasemi, H.R.; Hu, M.; Zhang, H.C. Determining and forecasting drought susceptibility in southwestern Iran using multi-criteria decision-making (MCDM) coupled with CA-Markov model. *Sci. Total. Environ.* **2021**, *781*, 146703. [CrossRef]
35. Zhao, M.M.; He, Z.B.; Du, J.; Chen, L.F.; Lin, P.F.; Fang, S. Assessing the effects of ecological engineering on carbon storage by linking the CA-Markov and InVEST models. *Ecol. Indic.* **2019**, *98*, 19–38. [CrossRef]
36. Liu, Y.; Zhang, J.; Zhou, D.M.; Ma, J.; Dang, R.; Ma, J.J.; Zhu, X.Y. Temporal and spatial variation of carbon storage in the Shule River Basin based on InVEST model. *Acta Ecol. Sinica* **2021**, *41*, 4052–4065. [CrossRef]
37. Rimal, B.; Keshtkar, H.; Sharma, R.; Stork, N.; Rijal, S.; Kunwar, R. Simulating urban expansion in a rapidly changing landscape in eastern Tarai, Nepal. *Environ. Monit. Assess.* **2019**, *191*, 255. [CrossRef]
38. Qian, W.Y.; Guan, W.H.; Huang, X.J. Assessing the Potential Impact of Land Use on Carbon Storage Driven by Economic Growth: A Case Study in Yangtze River Delta Urban Agglomeration. *Int. J. Environ. Res. Public Health* **2021**, *18*, 11924. [CrossRef]
39. Cai, W.B.; Peng, W.T. Exploring Spatiotemporal Variation of Carbon Storage Driven by Land Use Policy in the Yangtze River Delta Region. *Land* **2021**, *10*, 1120. [CrossRef]
40. Li, Y.G.; Liu, W.; Feng, Q.; Zhu, M.; Yang, L.S.; Zhang, J.T. Effects of land use and land cover change on soil organic carbon storage in the Hexi regions, Northwest China. *J. Environ. Manag.* **2022**, *312*, 114911. [CrossRef]
41. Liu, F.; Wu, H.Y.; Zhao, Y.G.; Li, D.C.; Yang, J.L.; Song, X.D.; Shi, Z.; Zhu, A.X.; Zhang, G.L. Mapping high resolution National Soil Information Grids of China. *Sci. Bull.* **2021**, *67*, 328–340. [CrossRef]

42. Liu, L.J.; Liang, Y.J.; Hashimoto, S. Integrated assessment of land-use/coverage changes and their impacts on ecosystem services in Gansu province, northwest China: Implications for sustainable development goals. *Sustain. Sci.* **2020**, *15*, 297–314. [CrossRef]
43. Wen, X.; Wu, X.; Meng, G. Spatiotemporal variability of temperature and precipitation in Gansu province (Northwest China) during 1951–2015. *Atmos. Res.* **2017**, *197*, 132–149. [CrossRef]
44. Lu, H.; Dong, J.R.; He, S.J.; Xie, Y.W. Vegetation change trend and persistence analysis of the mountainoasis-desert system in Hexi region from 2000 to 2017. *J. Lanzhou Univ. Nat. Sci.* **2021**, *57*, 99–108. [CrossRef]
45. Lai, L.; Huang, X.J.; Yang, H.; Chuai, X.W.; Zhang, M.; Zhong, T.Y.; Chen, Z.G.; Chen, Y.; Wang, X.; Thompson, J.R. Carbon emissions from land-use change and management in China between 1990 and 2010. *Sci. Adv.* **2016**, *2*, e1601063. [CrossRef]
46. Liang, Y.J.; Liu, L.J.; Huang, J.J. Integrating the SD-CLUE-S and InVEST models into assessment of oasis carbon storage in northwestern China. *PLoS ONE* **2017**, *12*, e0172494. [CrossRef]
47. Li, K.M.; Cao, J.J.; Adamowski, J.F.; Biswas, A.; Zhou, J.J.; Liu, Y.J.; Zhang, Y.K.; Liu, C.F.; Dong, X.G.; Qin, Y.L. Assessing the effects of ecological engineering on spatiotemporal dynamics of carbon storage from 2000 to 2016 in the Loess Plateau area using the InVEST model: A case study in Huining County, China. *Environ. Dev.* **2021**, *39*, 100641. [CrossRef]
48. Spawn, S.A.; Gibbs, H.K. *Global Aboveground and Belowground Biomass Carbon Density Maps for the Year 2010*; ORNL DAAC: Oak Ridge, TN, USA, 2020. [CrossRef]
49. Fang, X.; Zhang, C.; Zhang, Y.N.; Kang, J.F. A Dataset of Organic Carbon Storage and Carbon Dynamic in rid and Semiarid China from 1980 to 2014 [DS/OL]. Science Data Bank. 2018. Available online: https://www.scidb.cn/en/detail?dataSetId=633694461100032002 (accessed on 18 October 2021). [CrossRef]
50. Spawn, S.A.; Sullivan, C.C.; Lark, T.J.; Gibbs, H.K. Harmonized global maps of above and belowground biomass carbon density in the year 2010. *Sci. Data* **2020**, *7*, 112. [CrossRef]
51. Peng, S.Z.; Ding, Y.X.; Liu, W.Z.; Li, Z. 1 km monthly temperature and precipitation dataset for China from 1901 to 2017. *Earth Syst. Sci. Data* **2019**, *11*, 1931–1946. [CrossRef]
52. Peng, S.Z.; Ding, Y.X.; Wen, Z.M.; Chen, Y.M.; Cao, Y.; Ren, J.Y. Spatiotemporal change and trend analysis of potential evapotranspiration over the Loess Plateau of China during 2011–2100. *Agric. For. Meteorol.* **2017**, *233*, 183–194. [CrossRef]
53. Ding, Y.X.; Peng, S.Z. Spatiotemporal Trends and Attribution of Drought across China from 1901–2100. *Sustainability* **2020**, *12*, 477. [CrossRef]
54. Ding, Y.X.; Peng, S.Z. Spatiotemporal change and attribution of potential evapotranspiration over China from 1901 to 2100. *Theor. Appl. Climatol.* **2021**, *145*, 79–94. [CrossRef]
55. Peng, S. *1-km Monthly Precipitation Dataset for China (1901–2020)*; National Tibetan Plateau Data Center, Northwest A&F University: Xianyang, China, 2020. [CrossRef]
56. Peng, S. *1 km Multi-Scenario and Multi-Model Monthly Precipitation Data for China in 2021–2100*; National Tibetan Plateau Data Center, Northwest A&F University: Xianyang, China, 2022. [CrossRef]
57. Chen, S.P.; Wang, W.T.; Xu, W.T.; Wang, Y.; Wan, H.W.; Chen, D.M.; Tang, Z.Y.; Tang, X.L.; Zhou, G.Y.; Xie, Z.Q.; et al. Plant diversity enhances productivity and soil carbon storage. *Proc. Natl. Acad. Sci. USA* **2018**, *115*, 4027–4032. [CrossRef]
58. Fang, J.Y.; Yu, G.R.; Liu, L.L.; Chapin, F.S. Climate change, human impacts, and carbon sequestration in China. *Proc. Natl. Acad. Sci. USA* **2018**, *115*, 4015–4020. [CrossRef] [PubMed]
59. Yang, X.L.; Li, W.T.; Ren, L.L.; Gao, T.; Ma, H.J. Simulation of the response of blue and green water to land use change in the Weihe River Basin. *Trans. Chin. Soc. Agric. Eng.* **2021**, *37*, 268–276. [CrossRef]
60. Setturu, B.; Ramachandra, T.V. Modeling Landscape Dynamics of Policy Interventions in Karnataka State, India. *J. Geovis. Spat. Anal.* **2021**, *5*, 22. [CrossRef]
61. Piyathilake, I.D.U.H.; Udayakumara, E.P.N.; Ranaweera, L.V.; Gunatilake, S.K. Modeling predictive assessment of carbon storage using InVEST model in Uva province, Sri Lanka. *Model. Earth Syst. Environ.* **2021**, *8*, 2213–2223. [CrossRef]
62. Zhu, W.B.; Zhang, J.J.; Cui, Y.P.; Zhu, L.Q. Ecosystem carbon storage under different scenarios of land use change in Qihe catchment, China. *J. Geogr. Sci.* **2020**, *30*, 1507–1522. [CrossRef]
63. Liu, Z.P.; Shao, M.A.; Wang, Y.Q. Effect of environmental factors on regional soil organic carbon stocks across the Loess Plateau region, China. *Agric. Ecosyst. Environ.* **2011**, *142*, 184–194. [CrossRef]
64. Ashraf, S.; Ali, M.; Shrestha, S.; Hafeez, M.A.; Moiz, A.; Sheikh, Z.A. Impacts of climate and land-use change on groundwater recharge in the semi-arid lower Ravi River basin, Pakistan. *Groundw. Sustain. Dev.* **2022**, *17*, 100743. [CrossRef]
65. Tang, X.L.; Zhao, X.; Bai, Y.F.; Zhou, G.Y. Carbon pools in China's terrestrial ecosystems: New estimates based on an intensive field survey. *Proc. Natl. Acad. Sci. USA* **2018**, *115*, 4021–4026. [CrossRef]
66. Li, H.W.; Wu, Y.P.; Chen, J.; Zhao, F.B.; Wang, F.; Sun, Y.Z.; Zhang, G.C.; Qiu, L.J. Responses of soil organic carbon to climate change in the Qilian Mountains and its future projection. *J. Hydrol.* **2021**, *596*, 126110. [CrossRef]
67. Guan, J.H.; Du, S.; Cheng, J.M.; Wu, C.R.; LI, G.Q.; Deng, L.; Zhang, J.G.; He, Q.Y.; Shi, W.Y. Current stocks and rate of sequestration of forest carbon in Gansu province, China. *Chin. J. Plant Ecol.* **2016**, *40*, 304–317. [CrossRef]
68. Cheng, K.; Pan, G.X. "Four Per Mille Initiative: Soils for Food Security and Climate" Challenges and strategies for China's Action. *Clim. Change Res.* **2016**, *12*, 457–464. [CrossRef]
69. Liu, W.J.; Su, Y.Z.; Yang, R.; Wang, X.F.; Yang, X. Land use effects on soil organic carbon, nitrogen and salinity in saline-alkaline wetland. *Sci. Cold Arid. Reg.* **2010**, *2*, 263–270.

70. Li, Q.G.; Wang, L.C.; Gul, H.N.; Li, D. Simulation and optimization of land use pattern to embed ecological suitability in an oasis region: A case study of Ganzhou district, Gansu province, China. *J. Environ. Manag.* **2021**, *287*, 112321. [CrossRef]
71. Fewster, R.E.; Morris, P.J.; Ivanovic, R.F.; Swindles, G.T.; Peregon, A.M.; Smith, C.J. Imminent loss of climate space for permafrost peatlands in Europe and Western Siberia. *Nat. Clim. Chang.* **2022**, *12*, 373–379. [CrossRef]
72. Koch, A.; Kaplan, J.O. Tropical forest restoration under future climate change. *Nat. Clim. Chang.* **2022**, *12*, 279–283. [CrossRef]
73. Shi, H.; Tian, H.; Pan, N.; Reyer, C.P.O.; Ciais, P.; Chang, J.; Forrest, M.; Frieler, K.; Fu, B.; Gädeke, A.; et al. Saturation of global terrestrial carbon sink under a high warming scenario. *Glob. Biogeochem. Cycles* **2021**, *35*, e2020GB006800. [CrossRef]